Numerical simulation of an Alaska 1964-type tsunami with application to Boundary Bay in the southern Strait of Georgia under future global sea level conditions

Isaac V. Fine and Richard E. Thomson

Fisheries and Oceans Canada
Institute of Ocean Sciences
9860 West Saanich Road
Sidney, BC V8L 4B2

2026

Canadian Technical Report of
Hydrography and Ocean Sciences 415

Fisheries and Oceans Canada | Pêches et Océans Canada

Canada

Canadian Technical Report of Hydrography and Ocean Sciences

Technical reports contain scientific and technical information of a type that represents a contribution to existing knowledge, but which is not normally found in the primary literature. The subject matter is generally related to programs and interests of the Oceans and Science sectors of Fisheries and Oceans Canada.

Technical reports may be cited as full publications. The correct citation appears above the abstract of each report. Each report is abstracted in the data base Aquatic Sciences and Fisheries Abstracts.

Technical reports are produced regionally but are numbered nationally. Requests for individual reports will be filled by the issuing establishment listed on the front cover and title page. Regional and headquarters establishments of Ocean Science and Surveys ceased publication of their various report series as of December 1981. A complete listing of these publications and the last number issued under each title are published in the Canadian Journal of Fisheries and Aquatic Sciences, Volume 38: Index to Publications 1981. The current series began with Report Number 1 in January 1982.

Rapport technique canadien sur l'hydrographie et les sciences océaniques

Les rapports techniques contiennent des renseignements scientifiques et techniques qui constituent une contribution aux connaissances actuelles mais que l'on ne trouve pas normalement dans les revues scientifiques. Le sujet est généralement rattaché aux programmes et intérêts des secteurs des Océans et des Sciences de Pêches et Océans Canada.

Les rapports techniques peuvent être cités comme des publications à part entière. Le titre exact figure au-dessus du résumé de chaque rapport. Les rapports techniques sont résumés dans la base de données Résumés des sciences aquatiques et halieutiques.

Les rapports techniques sont produits à l'échelon régional, mais numérotés à l'échelon national. Les demandes de rapports seront satisfaites par l'établissement auteur dont le nom figure sur la couverture et la page de titre.

Les établissements de l’ancien secteur des Sciences et Levés océaniques dans les régions et à l'administration centrale ont cessé de publier leurs diverses séries de rapports en décembre 1981. Vous trouverez dans l'index des publications du volume 38 du Journal canadien des sciences halieutiques et aquatiques, la liste de ces publications ainsi que le dernier numéro paru dans chaque catégorie. La nouvelle série a commencé avec la publication du rapport numéro 1 en janvier 1982.

Canadian Technical Report of
Hydrography and Ocean Sciences 415

2026

NUMERICAL SIMULATION OF AN ALASKA 1964-TYPE TSUNAMI WITH APPLICATION TO BOUNDARY BAY IN THE SOUTHERN STRAIT OF GEORGIA UNDER FUTURE GLOBAL SEA LEVEL CONDITIONS

By

Isaac V. Fine and Richard E. Thomson

Fisheries and Oceans Canada
Institute of Ocean Sciences
9860 West Saanich Road
Sidney, BC V8L 4B2

Cat. No. Fs 97-18/415E-PDF ISBN 978-0-660-99247-1 ISSN 1488-5417

Correct citation for this publication:

Fine, I.V., and Thomson, R.E. 2026. Numerical simulation of an Alaska 1964-type tsunami with application to Boundary Bay in the southern Strait of Georgia under future global sea level conditions. Can. Tech. Rep. Hydrogr. Ocean Sci. 415: v + 51 p.

CONTENTS

ABSTRACT

Fine, I.V., and Thomson, R.E. 2026. Numerical simulation of an Alaska 1964-type tsunami with application to Boundary Bay in the southern Strait of Georgia under future global sea level conditions. Can. Tech. Rep. Hydrogr. Ocean Sci. 415: v + 51 p.

Estimation of the tsunami risk to the British Columbia coast from an event similar to the devastating Alaska 1964 magnitude 9.2 earthquake and tsunami is especially important for broad, low-lying marine areas of the province such as Boundary Bay. This risk is expected to increase as global sea levels continue to rise through the effects of global warming. A state-of-the-art numerical model based on newly available high-resolution bathymetric and topographic data was used to estimate the impact of an Alaska 1964-type tsunami on Boundary Bay under three future sea level rise scenarios: Scenario-1, a 0.5 m global sea level rise; Scenario-2, a 1 m global sea level rise; and Scenario-3, a 2 m global sea level rise. Each scenario is obtained by downscaling of regional sea level rise predictions that take into account local tectonic movement. The main findings of the modeling are: (1) Scenarios 2 and 3 require an increase in the height of the dike system situated along the northern shore of Boundary Bay and along the Serpentine and Nicomekl rivers. Without these changes, flooding would occur before any tsunami waves arrive in the area; (2) the tsunami at Boundary Bay will reach 0.45 m above the tidal level at the time of the wave arrivals for all sea level rise scenarios; (3) the distribution of tsunami wave amplitudes in Boundary Bay will be non-uniform, with the highest waves impacting Mud Bay and Drayton Harbor; and (4) the tsunami will induce moderate currents at the entrance to Drayton Harbor (up to 1.5 m/s), at the mouth of the Nicomekl River (up to 0.8 m/s) and at the mouth of the Campbell River (up to 0.7 m/s). With sea level rise, current speeds increase in the entrances to the rivers, but decrease at the entrance to Drayton Harbor.

RÉSUMÉ

Fine, I.V., and Thomson, R.E. 2026. Numerical simulation of an Alaska 1964-type tsunami with application to Boundary Bay in the southern Strait of Georgia under future global sea level conditions. Can. Tech. Rep. Hydrogr. Ocean Sci. 415: v + 51 p.

L'estimation du risque de tsunami sur la côte de la Colombie-Britannique, découlant d'un événement similaire au séisme et au tsunami dévastateurs de magnitude 9,2 survenus en Alaska en 1964, est particulièrement importante pour les vastes zones marines basses de la province, comme la baie Boundary. Ce risque devrait s'accroître avec l'élévation continue du niveau de la mer sous l'effet du réchauffement climatique. Un modèle numérique de pointe, basé sur des données bathymétriques et topographiques à haute résolution récemment disponibles, a été utilisé pour estimer l'impact d'un tsunami de type Alaska de 1964 sur la baie Boundary selon trois scénarios d'élévation du niveau de la mer: scénario 1, élévation globale de 0,5 m ; scénario 2, élévation globale de 1 m ; et scénario 3, élévation globale de 2 m. Chaque scénario est obtenu par réduction d'échelle des prévisions régionales d'élévation du niveau de la mer, qui tiennent compte des mouvements tectoniques locaux. Les principaux résultats de la modélisation sont les suivants: (1) Les scénarios 2 et 3 nécessitent une augmentation de la hauteur du système de digues situé le long de la rive nord de Boundary Bay et des rivières Serpentine et Nicomekl. Sans ces modifications, les inondations surviendraient avant l'arrivée des vagues de tsunami dans la région; (2) le tsunami à Boundary Bay atteindra 0,45 m au-dessus du niveau de la marée au moment de l'arrivée des vagues, quel que soit le scénario d'élévation du niveau de la mer; (3) la distribution des amplitudes des vagues de tsunami à Boundary Bay sera hétérogène, les vagues les plus hautes touchant Mud Bay et Drayton Harbor; et (4) le tsunami induira des courants modérés à l'entrée de Drayton Harbor (jusqu'à 1,5 m/s), à l'embouchure de la rivière Nicomekl (jusqu'à 0,8 m/s) et à l'embouchure de la rivière Campbell (jusqu'à 0,7 m/s). Avec l'élévation du niveau de la mer, la vitesse des courants augmente aux embouchures des rivières, mais diminue à l'entrée de Drayton Harbor.

The Strait of Georgia. Photo by Dave Hutchinson.

1. INTRODUCTION

The devastating tsunamis that have occurred in the last two decades, including the 2004 Sumatra, 2010 Chile and 2011 Tohoku events, highlight the potential threat of major seismically generated tsunamis to coastal communities in southern British Columbia (BC). Estimations of the tsunami risk to the British Columbia coast, especially from events similar to the devastating Alaska magnitude M_w 9.2 earthquake and the January 1700 magnitude M_w 9.0 Cascadia Subduction Zone earthquake, are of considerable importance for broad, low-lying areas of BC such as Boundary Bay. This risk is expected to increase as global sea levels continue to rise through the effects of global warming.

The Alaska earthquake of March 28, 1964 generated a catastrophic tsunami, the second greatest in the 20th century after the 1960 Chilean tsunami, with maximum wave heights of 20 m near the earthquake source region. A large number of landslides and submarine landslides were also initiated, resulting in local tsunami waves as high as 70 m (Lander, 1996). The magnitude M_w 9.2 earthquake, which was the strongest instrumentally recorded earthquake in the North Pacific and second in magnitude only to the M_w 9.5 Chilean earthquake in 1980, occurred in the vicinity of Prince

William Sound, leading to the widely used name of the "Prince William Sound Earthquake" (Spaeth and Berkman, 1967). Because of the event date (March 28), the earthquake and associated Pacific-wide tsunami are also called the "Good Friday Earthquake and Tsunami".

The 1964 tsunami was responsible for close to 130 deaths and about million dollars in damage in Alaska, Washington, California and Hawaii (Spaeth and Berkman, 1967; Lander, 1996; Stephenson et al., 2007). Several locations on the coast of British Columbia suffered major damage (Clague et al., 2003; Anderson and Gow, 2004; Stephenson et al., 2007), with the highest wave ever recorded in Canada occurring at Shields Bay on the west coast of Graham Island (Haida Gwaii). Here, a wave crest was reported to be 5.2 m above the spring high water, or 9.8 m above tidal datum. Most of the damage from the tsunami occurred in Port Alberni, where a wave reached 4.2 m above the spring-tide high water (Dunbar et al., 1991; Fine et al., 2008). Because of its exceptional characteristics, the 1964 Alaska tsunami is typically considered as a proxy for a major future tsunami along the Pacific coast of North America (Suleimani et al., 2013).

Several numerical models were constructed to simulate tsunami wave propagation from the 1964 event in the northeast Pacific Ocean (cf. Dunbar et al., 1991; Myers and Baptista, 2001). Although these studies were able to simulate the main features of the tsunami impact on the British Columbia Coast, a more detailed analysis based on recent high-resolution bathymetry and a more refined high-resolution source region of the uplift distribution was needed. These aspects of the modeling requirements were addressed in a previous study by Fine et al. (2018b), which forms the basis for the present report. Here, the goal is to examine the effects of global sea level rise over the next two centuries on tsunami waves arriving at the highly vulnerable Boundary Bay region in the southern Strait of Georgia from an Alaska 1964-type, M_w 9.2 earthquake. The results of study also provide valuable insight into the wave heights that would occur over a broad area of the south coast of British Columbia from such an event under ongoing global sea level rise conditions.

2. MODEL SETUP

2.1. NESTED GRID FORMULATION

Accurate numerical simulation of tsunami waves in the rapidly shoaling regions of the west coast of British Columbia requires setting up the model domain as a series of nested grids of ever finer spatial and temporal resolution. The use of nested grids and nested grid formulation was

described in Fine et al. (2018b). The parameters of the nested grids are described in Table 1. The domains of Grids 1 through 4 for present-day mean sea level conditions are shown in Figures 1 to 4, respectively.

Table 1. Parameters of the numerical grids used in the tsunami generation and propagation model. Grid extent is along the *x* (eastward) and *y* (northward) coordinate directions and is presented in degrees (°). Numerical grid cell sizes for Grids 2, 3 and 4 are roughly 270, 60 and 10 m, respectively. Columns 2,3 and 4 are presented as *x*,*y* values. DEM denotes the Digital Elevation Model provided by Ocean Networks Canada.

Grid No.	Extent (*x, y*) (degrees)	Array (number of grid points)	Cell size (degrees)	Source of data	Processing type
1	34.0, 16.0	1361, 961	0.025, 0.01667	GEBCO 2014 30 arc- seconds gridded data	Filtering and bilinear interpolation
2	6.595, 4.2	1261,1520	0.005, 0.00333	BC 3 arc-sec bathymetric DEM	Filtering and bilinear interpolation
3	0.74, 0.55	811, 889	0.0008333, 0.0005555	BB 1/9 arc second DEM	Filtering and interpolation
4	0.38, 0.20	2737, 2161	0.000138889, 0.0000925926	BB 1/9 arc second	Filtering and interpolation

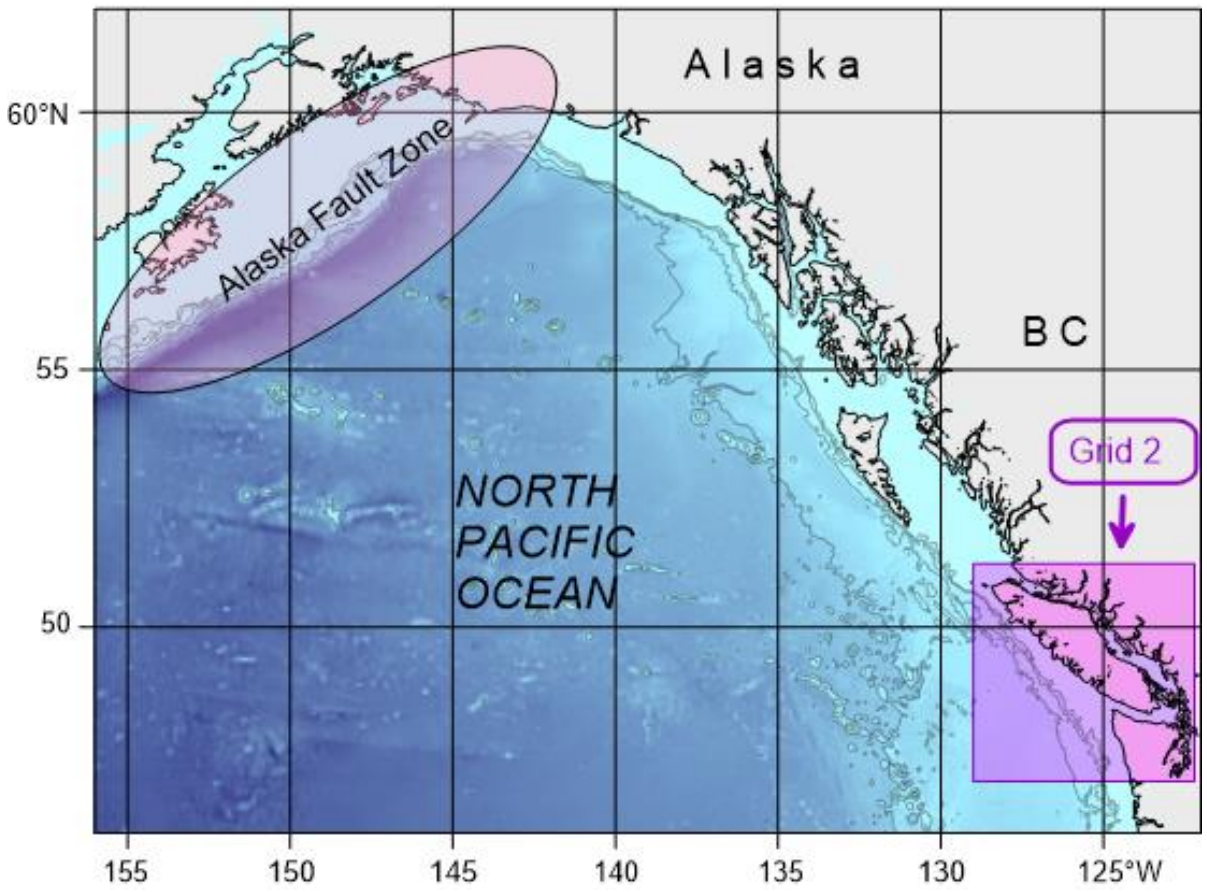

Figure 1. The region covered by the large-scale coarse grid numerical model for the northeast Pacific (Grid 1). Also shown is the Alaska Fault Zone that could generate tsunamis that impact the Boundary Bay region. The insert shows the location of the first nested grid (Grid 2), covering the coast of Vancouver Island, British Columbia, and northwest Washington State.

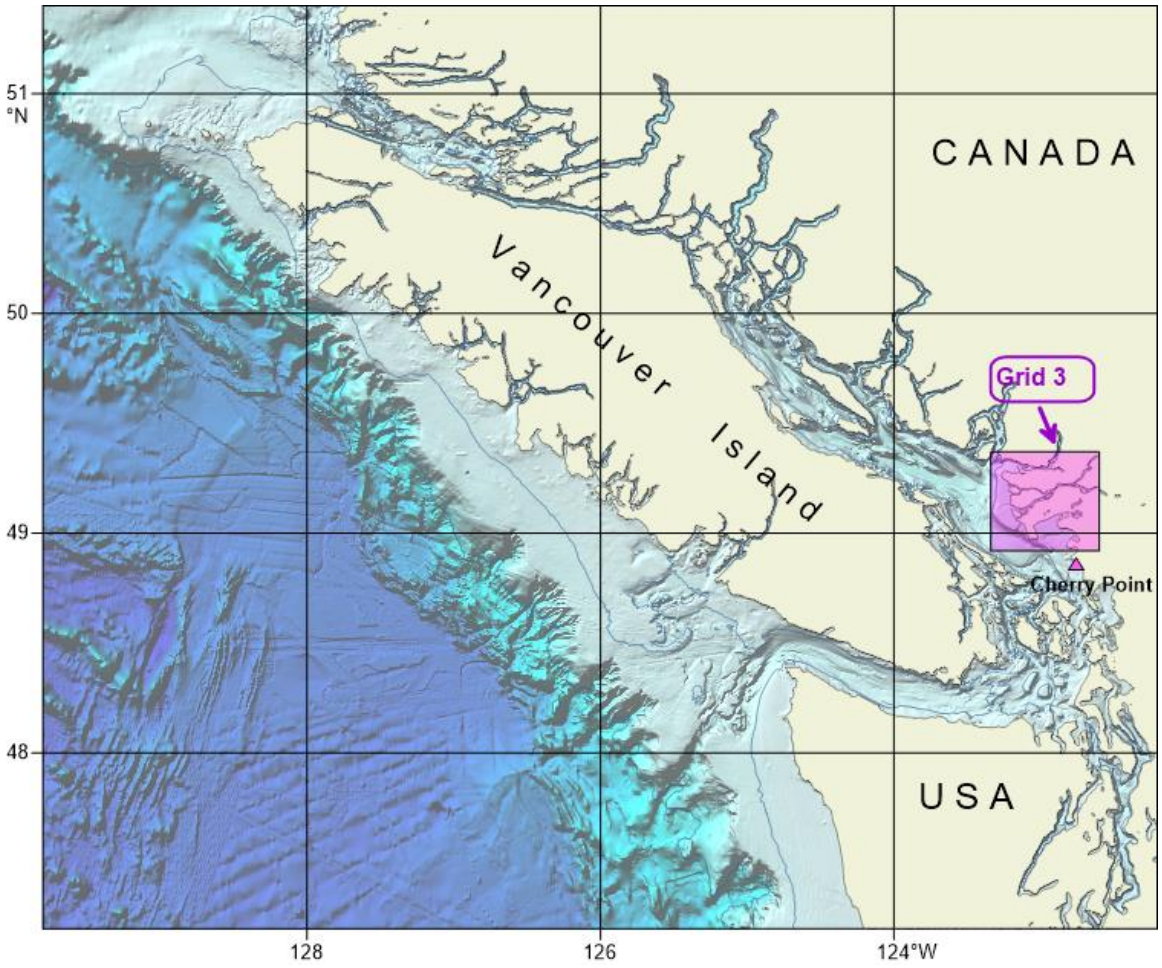

Figure 2. Vancouver Island and surrounding oceanic regions covered by the medium-scale bathymetric grid (Grid 2) for the southwest coast of British Columbia. The horizontal grid cell scales (x, y) for this region are approximately 370 m. The insert shows the boundaries and location of the second nested grid (Grid 3) covering the region of Metro Vancouver and Boundary Bay.

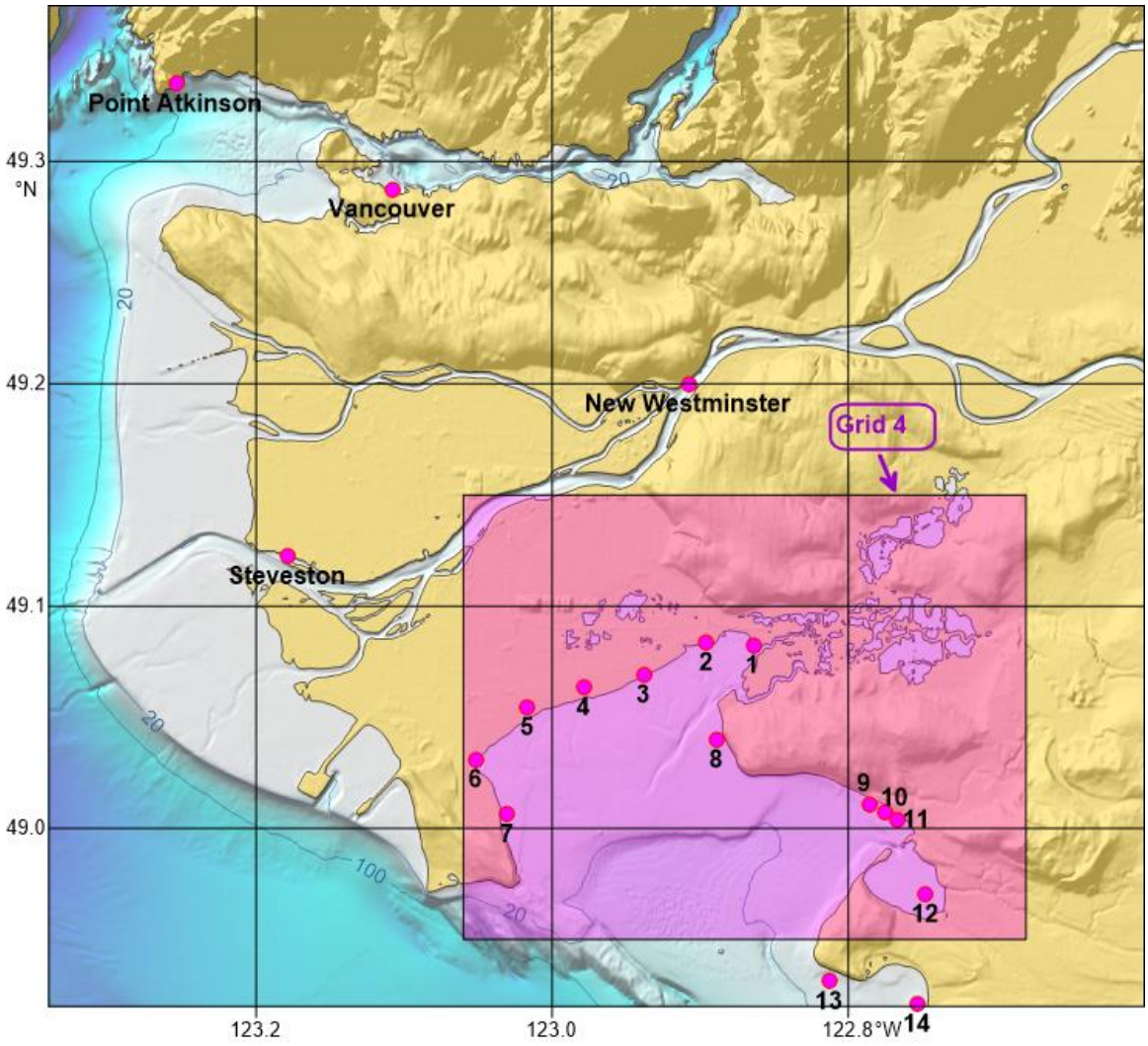

Figure 3. The coastal region covered by Grid 3, including the waters surrounding Greater (Metro) Vancouver. The *x*,*y* grid scales for this region are approximately 61 m and 62 m, respectively. Shown are the locations of the tide gauges (solid dots) and the model output sites (numbers 1-14). The area above mean sea level is shaded yellow. The insert shows the boundaries and location of the fourth nested grid (Grid 4) covering Boundary Bay.

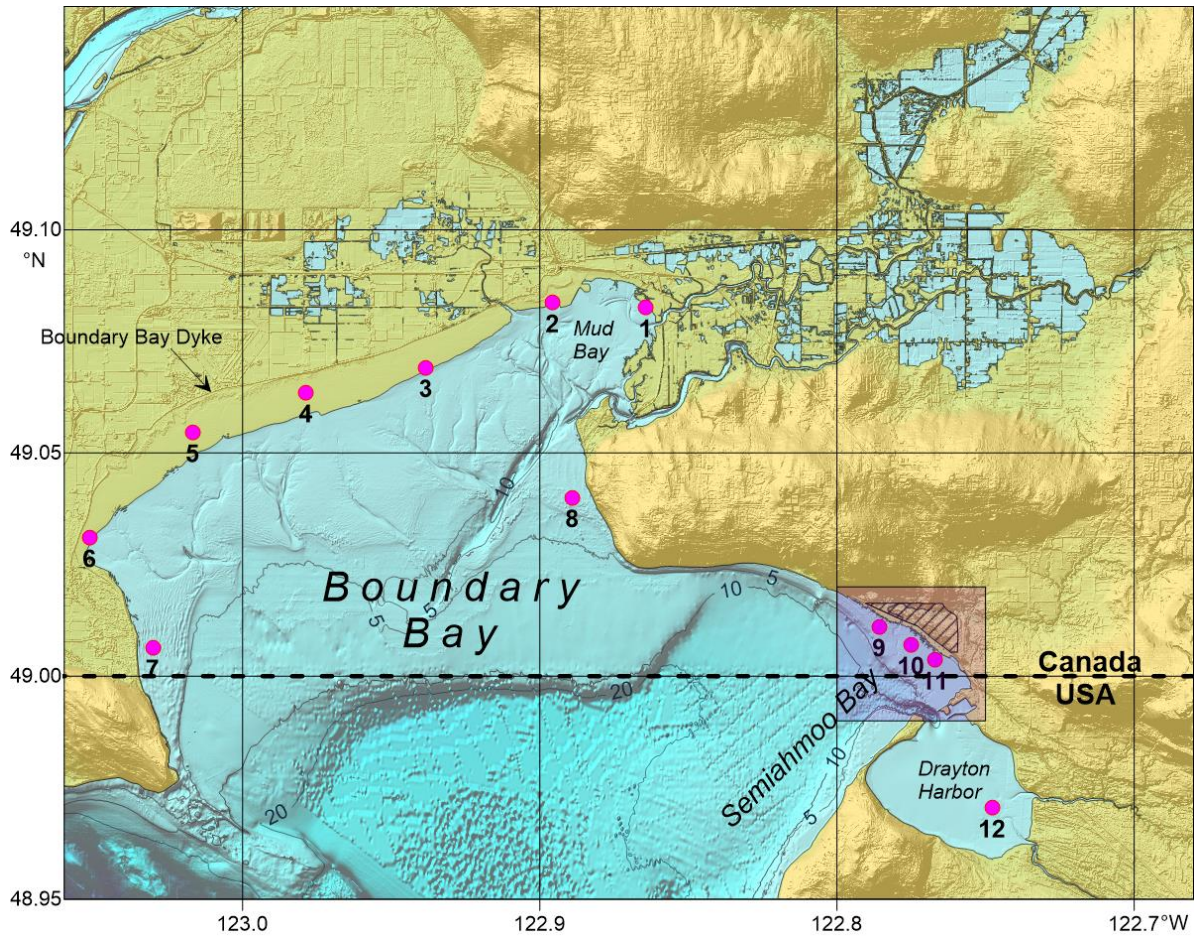

Figure 4. The region covered by Grid 4. The fine-scale bathymetric grid has adjusted topography for Boundary Bay, with grid scales (x,y) of approximately 10 m by 10 m. Also shown are the sites (numbers 1-12) for which tsunami wave records have been simulated. Depths, H, are in metres (m). The area above mean sea level is shaded in yellow. The hatched area denotes the location of the Semiahmoo, First Nations Reserve.

2.2. SEA LEVEL RISE SCENARIOS

We have considered three scenarios of sea level rise:

(a) *Scenario-1 (S1)*: The Median RCP8.5 scenario, which leads to an approximately 0.5 m rise in global sea level by 2080;

(b) *Scenario-2 (S2)*: The Upper RCP8.5 scenario, which leads to an approximately 1 m rise in global sea level by 2100;

(c) *Scenario-3 (S3)*: Extreme global sea level rise of 2 m by year 2200.

Details on the above scenarios are described in the **"**Tabulated Values of Relative Sea-level Projections in Canada and the Adjacent Mainland United States**"** (Geological Survey of Canada, Open File 7942, 2015). The digital data of sea level rise for the present study were downscaled into a nested grid model.

Maps of sea level rise for the three scenarios for Grid 2 of the modeled domains are shown in Figure 5. The distributions consist of sea level rise minima in the northern Strait of Georgia, as well as in the central and southern parts of the west coast of Vancouver Island. The highest rise is in the southern Strait of Georgia and eastern Juan de Fuca Strait. Differences in sea level rise are related to differences in local tectonic uplift.

Figures 6 and 7 show further downscaling of the original sea level rise values into the level 3 and level 4 modeling domains. It is clear that for sea level rise Scenario-2 (corresponding to a 1 m global sea level rise), part of the Greater Vancouver area will be below mean sea level. The situation is even more serious for Scenario-3, where significant parts of the area become below mean sea level and will need protection.

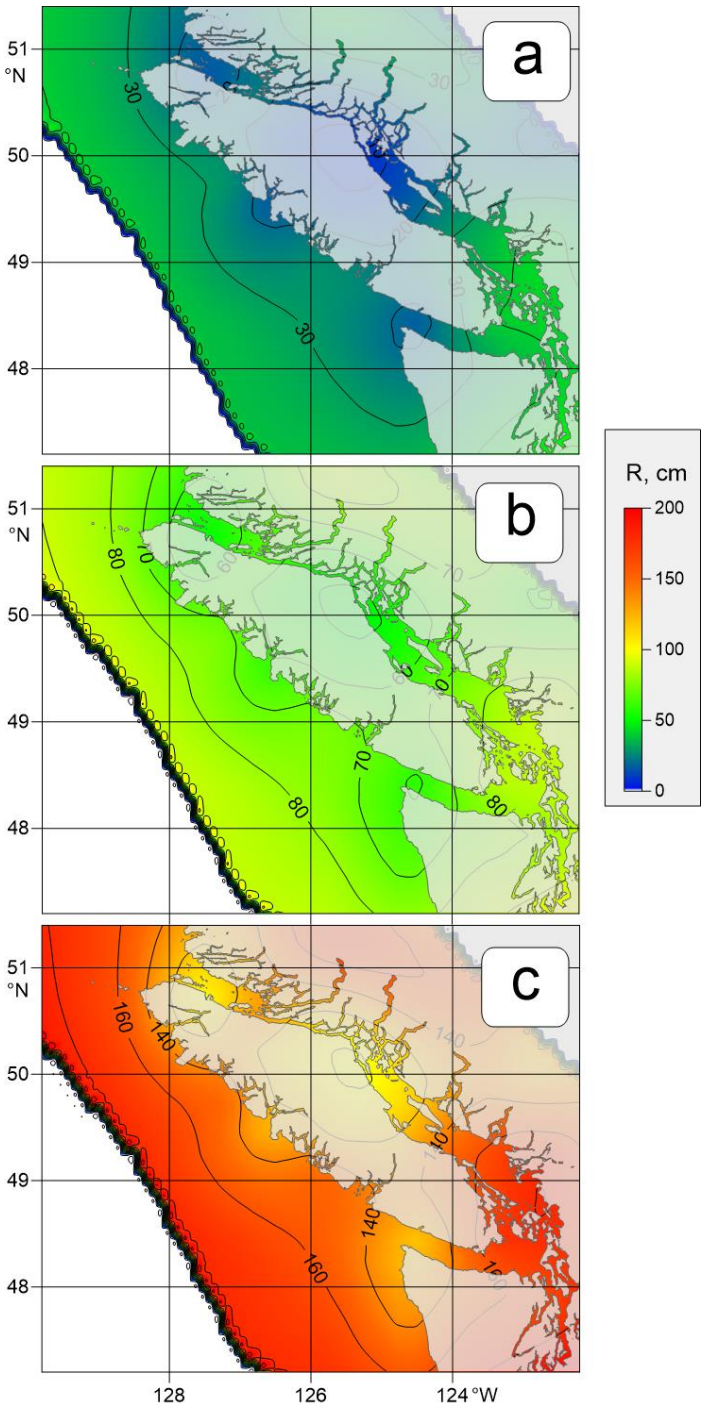

Figure 5. Sea level rise (R) distributions over the domain of Grid 2 of the model for: (a) a 0.5 m global rise for the median RCP8.5 Scenario-1 (S1); (b) a 1 m global rise for the upper RCP8.5 Scenario-2 (S2); and (c) a 2 m global rise for the year 2200 (Scenario-3; S3).

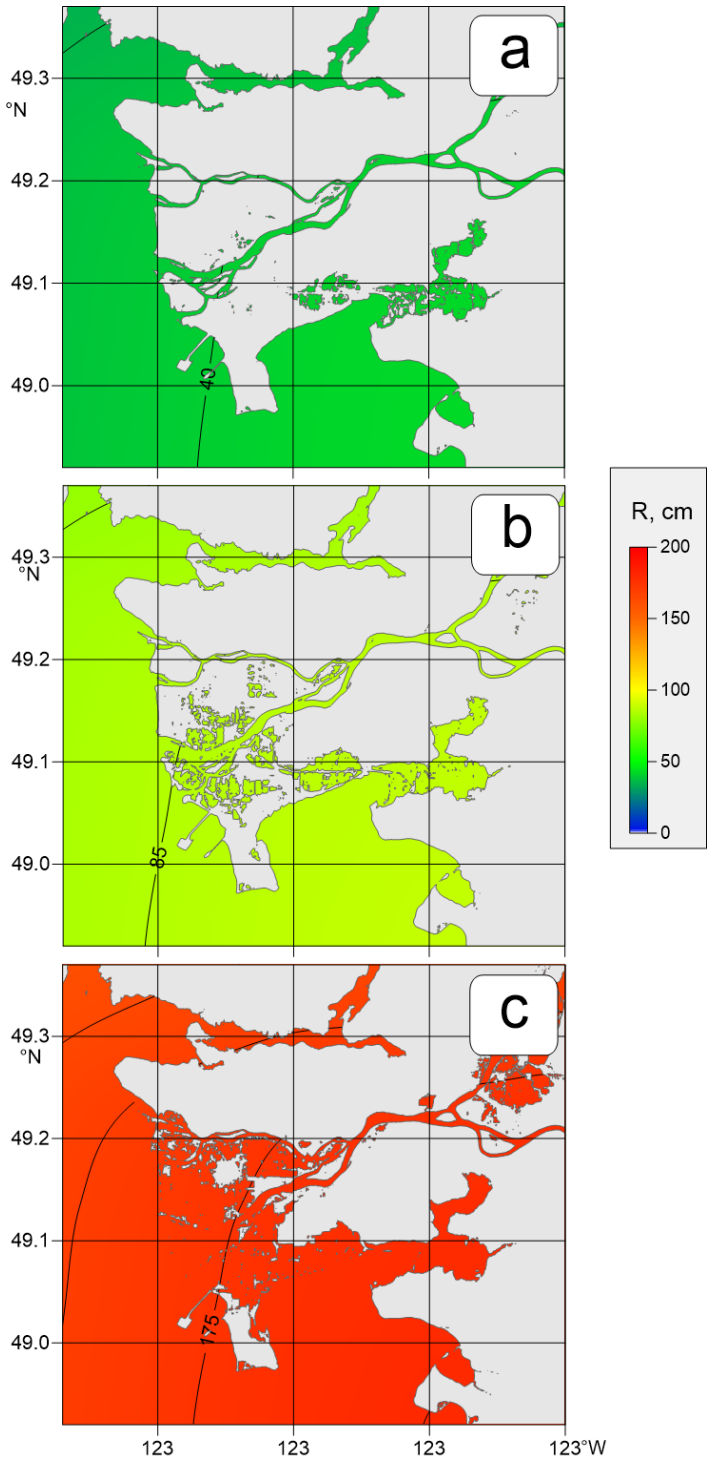

Figure 6. Sea level rise (R) distributions over the domain of Grid 3 of the model for: (a) a 0.5 m global rise for the upper RCP8.5 Scenario-1; (b) a 1 m global rise for the upper RCP8.5 Scenario-2); and (c) a 2 m global rise for the year 2200 (Scenario-3). The area above mean sea level is shown in grey.

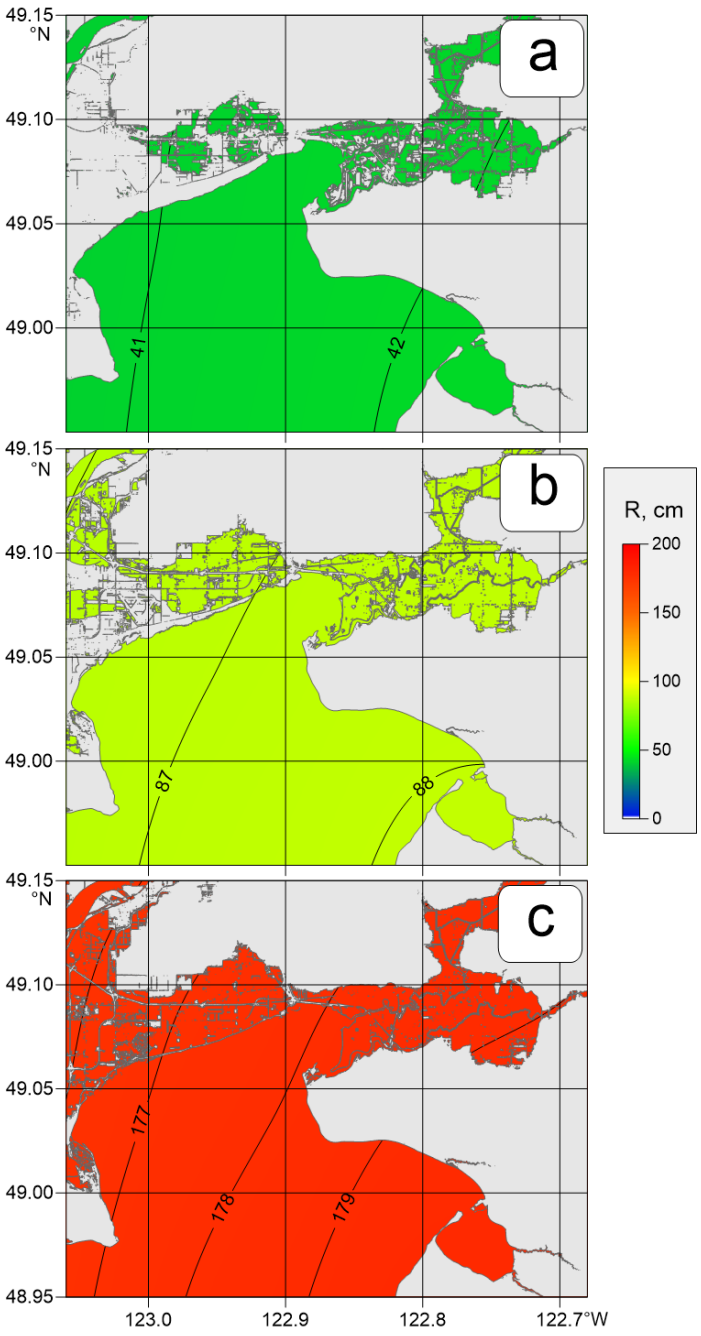

Figure 7. Sea level rise (*R*) distributions over the domain of Grid 4 of the model for: (a) a 0.5 m global rise for the median RCP8.5 Scenario-1; (b) a 1 m global rise for the upper RCP8.5 Scenario-2; and (c) a 2 m global rise for year 2200 corresponding to Scenario-3. The area above mean sea level is shown in grey.

2.3. DIKE HEIGHT IN BOUNDARY BAY

The shores of Boundary Bay are protected from flooding by a dike situated along the north-eastern side, around the northern coast, and along the north-western to eastern coastline. The dikes, which protect the low land in the coastal area, can be divided into three zones (Figure 8). In Zone A, the top of the dike is currently about 3 m above geodetic datum (see Figures 9 and 10). In Zone B, the northern segment, the top of the dike is roughly 3.5 m above geodetic datum (see Figures 9 and 11). Finally, in the north-western segment (Zone C), there is a series of dikes, which protect the land to the northwest of Boundary Bay from direct flooding from the bay, and from two rivers, the Serpentine and Nicomekl, whose shores are also protected with dikes on bi vary significantly, from 2.8 m to nearly 5 m above geodetic datum (see Figure 12 for the cross-sections and Figure 9 for the dike map). (Here, geodetic datum denotes Canadian Geodetic Vertical Datum, CGVD2013).

It is clear that, for the SLR-2 Scenario (sea level rise for the upper case of RCP8.5 by 2100), the current dike level only marginally protects low-lying areas. This is because the maximum tidal level (Large Tide) is about 60-65 cm above higher high water mean tide (HHWMT). In case of Scenario-3, even the HHWMT level will be above the present level of the dike. So, our model cannot start normally for future sea level conditions as flooding will begin at the start of the model run, well before any tsunami waves arrive in the area.

To avoid initial flooding under Scenario-3 conditions, we increased the top of the dike by about 1.5 m. The dike-rise procedure was performed in three stages. During the first sage, the existing dike axis (the line marking the top of the dike) was digitized using special software having an accuracy of the order of the grid size (about 10 m). During the second stage, a moving “dump truck” algorithm was applied, with small steps of about 1 m for each increment along the dike path. The algorithm starts by raising the end of the dike by 1.5 m; it then raises the dike by artificially adding “material” (i.e., adding elevation) to the top of the dike. At each 1-m step, the algorithm creates a new dike topography having the shape of a round two-dimensional (2D) Gaussian distribution with a height of 1.5 m and its centre at the current centre position on the dike path. The Gaussian radius was set to 40 m. The Gaussian height at the new position was then compared to the modified dike height at the previous step. A new Gaussian shape was then created at the new site by allocating to the new site the highest value of the previously constructed height and the current site. Then the “dump truck” was advanced along the dike path to the next location. Finally, a near-ideal “upgraded”

dike with a constant height was created along the whole path. The upgraded dike heights are shown as dashed lines in Figures 10 to 12.

Finally, at the third stage, the upgraded dike bathymetry was added to the existing model bathymetry to create updated bathymetry for Grid 4 for future modeling use. Figures 10, 11, and 12 shows the existing and updated cross-section of the bathymetry along different lines.

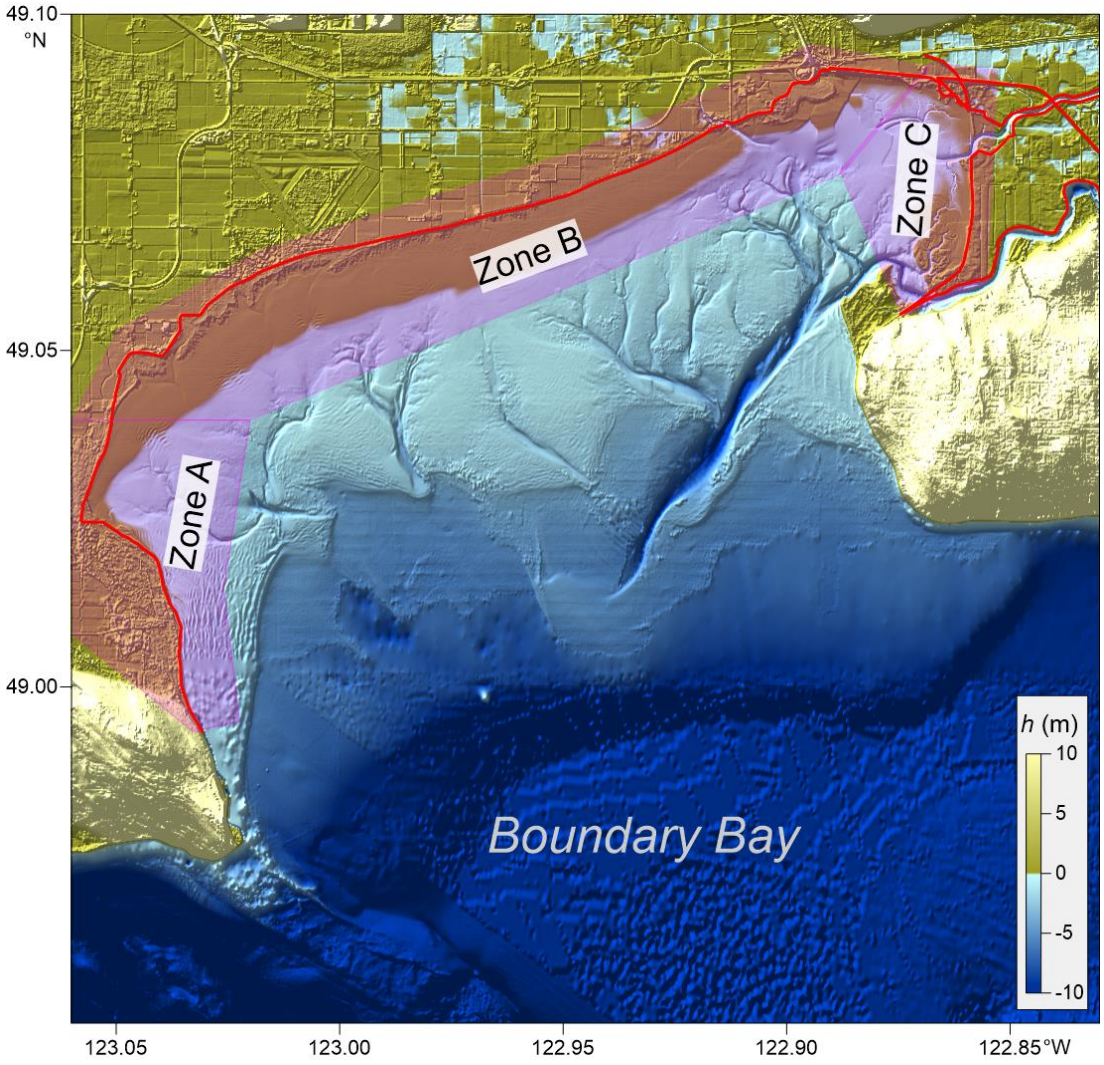

Figure 8. Map of Boundary Bay created using the bathymetric map for the Grid 4 domain. Shown are the locations of the dikes and the dike zones; *h* denotes the elevation.

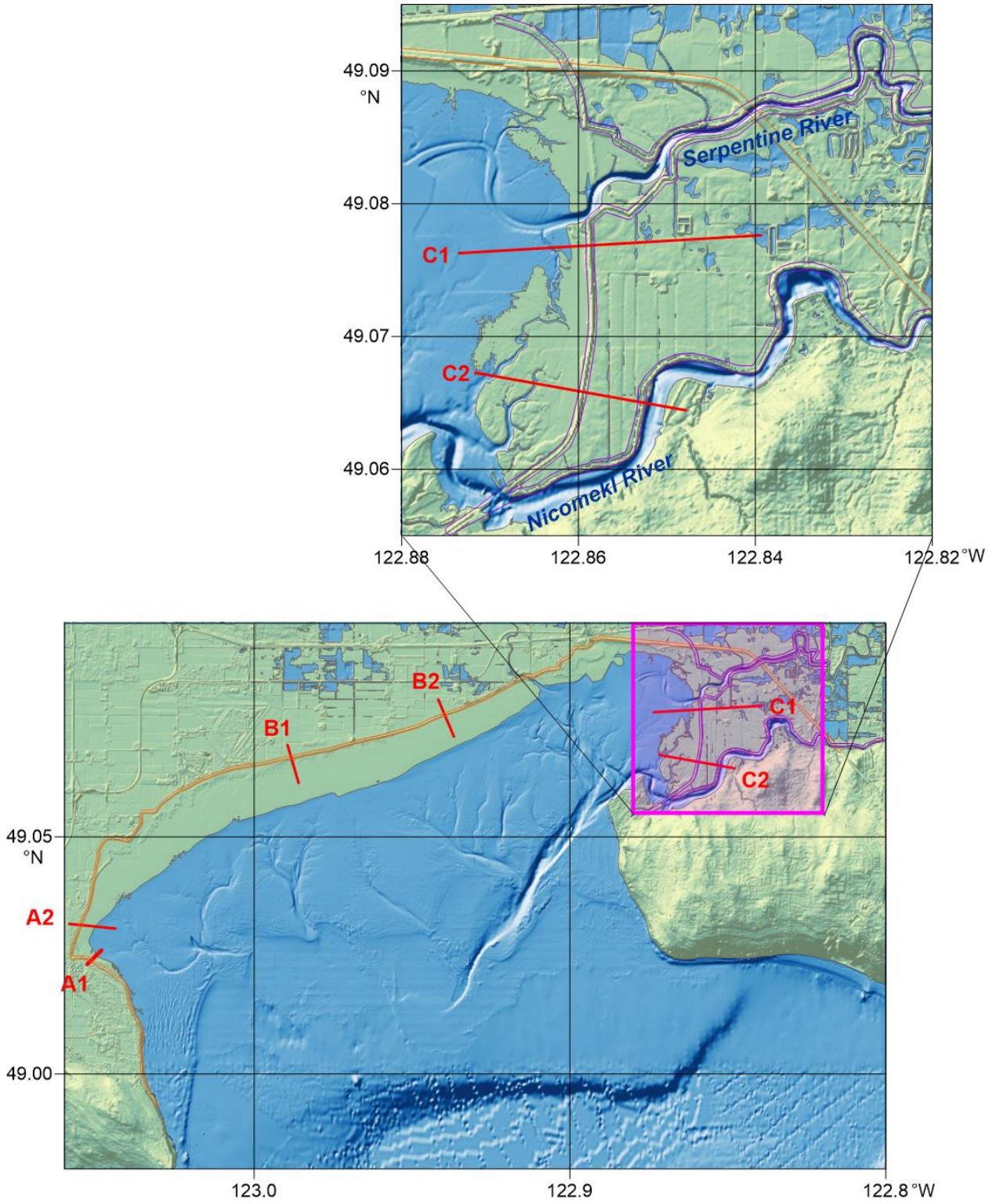

Figure.9. Map of Boundary Bay showing the locations of the dikes and locations of the cross-sections across the dike. The insert shows the location of the dikes along the rivers.

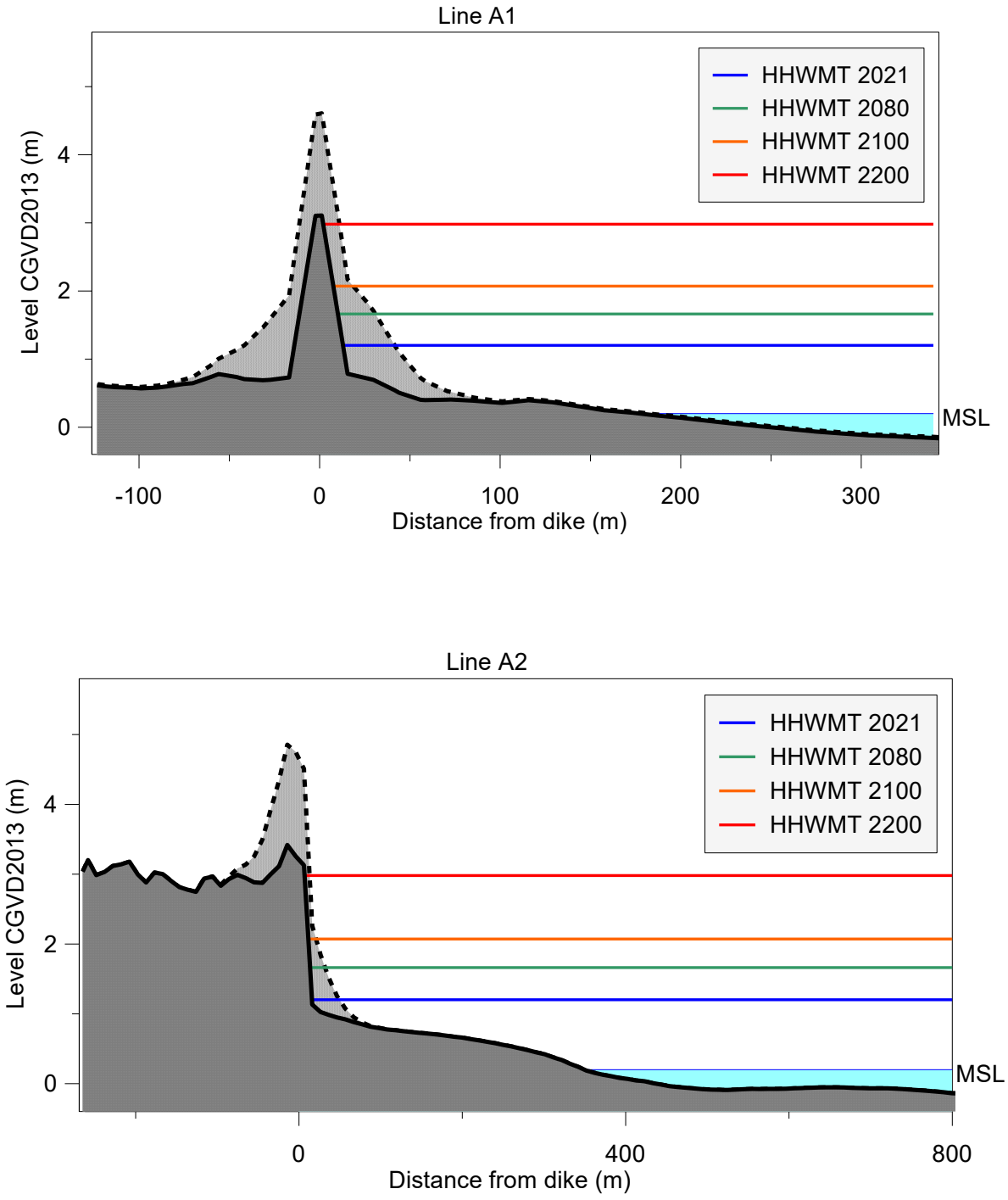

Figure 10. Cross-sections along lines A1 (upper panel) and A2 (lower panel). See Figure 9 for the locations of the lines. Also shown are the positions of present-day higher high water mean tide (HHWMT) (blue lines) and HHWMT for different sea level rise scenarios. The solid line and darkly shaded region denote the existing seabed and dike; the dashed line and lightly shaded region denote a proposed future dike.

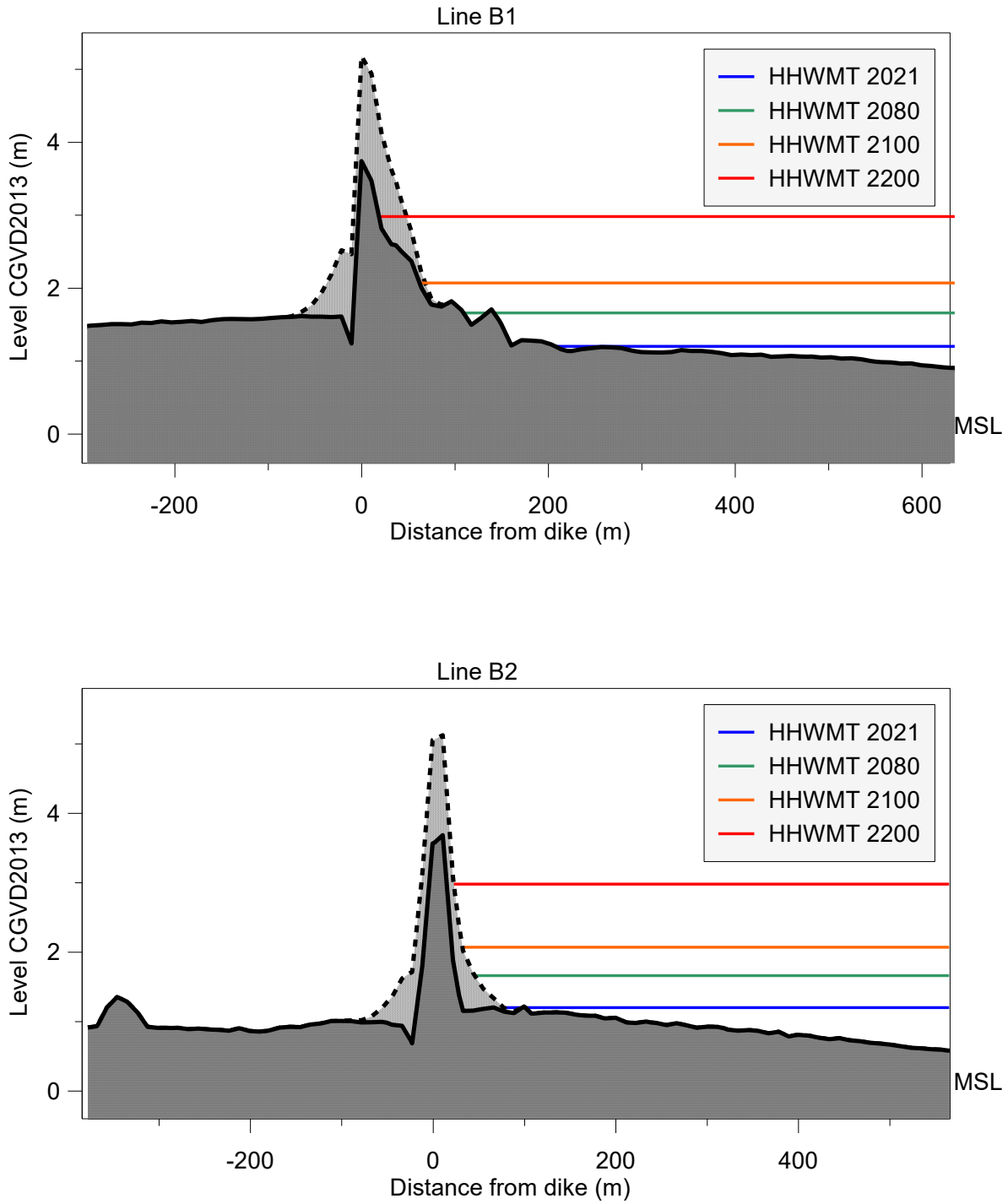

Figure 11. Cross-sections along lines B1 (upper panel) and B2 (lower panel). See Figure 9 for the locations of the lines. Also shown are the position of the present-day higher high water mean tide (HHWMT) (blue lines) and HHWMT for different sea level rise scenarios. The solid line and darkly shaded region denote the existing seabed and dike; the dashed line and lightly shaded region denote a proposed future dike.

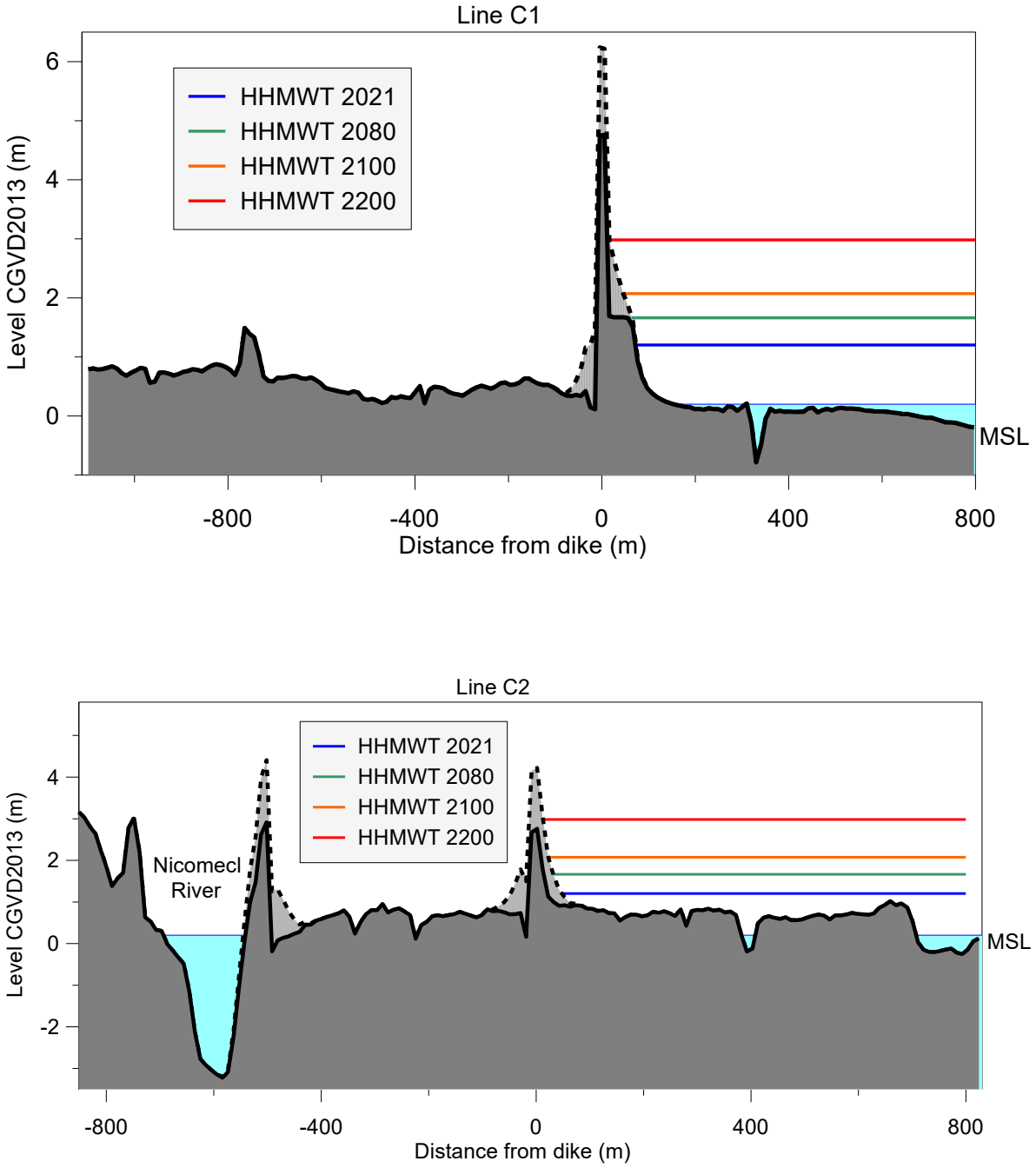

Figure 12. As for Figure 11 but for lines C1 (upper panel) and C2 (lower panel).

2.4. MODEL REFERENCE LEVEL

Model simulations are generally conducted for tsunami arrival times that coincide with high water conditions corresponding to the Canadian Vertical Datum of higher high water mean tide (HHWMT). The National Tsunami Hazard Mapping Program of 2010 (Nikolsky et al., 2013) recommends that inundation maps be computed using high tide as the initial condition for modelling. Alaska University uses Mean Higher High Water (MHHW) as the initial condition (Suleimani et al., 2013), while the Washington State inundation map was created using Mean High Water (MHW) for initial conditions (Eungard et al., 2018. The Canadian standard HHWMT is close to the US standard MHHW and has been used for many tsunami modelling projects in BC for Victoria (AECOM, 2013), for Victoria and Seal Cove (Fine et al., 2018a, 2018b), and for Prince Rupert (The City of Prince Rupert Tsunami Flooding Risk Assessment, 2019). Accordingly, to present values of highest risk, maps of maximum tsunami wave height and current speed in this report are referenced to HHMWT rather than to the mean tide or to a geodetic reference.

Higher High Water Mean Tide (HHWMT) is used as the primary reference level for most modelling results. For the Boundary Bay area, the closest permanent tide gauges are at Point Atkinson and Vancouver (Canadian Hydrographic Services) to the north and at Cherry Point (NOAA) to the south. HHWMT is 1.30 m above Mean Sea Level (MSL) at Point Atkinson and 1.32 m above MSL at Vancouver; in comparison, MHHW used in the US is 1.18 m above MSL at Point Atkinson (see Table 2 below). For convenience, a common reference value of 1.2 m is added throughout the region for the tsunami modelling. Mean Sea Level (MSL) is 0.18-0.19 m above the Canadian geodetic datum CGVD2013 (Table 2).

For the each of three sea level rise Scenarios, the computed sea level rise values for each grid (see Figures 5, 6 and 7) were added to the bathymetry of Grids 2, 3 and 4, in addition to the Higher High Water values. Grid 4 has a modified dike, whose height was increased by 1.5 m (see Section 2.3 for details). Grid 1 was unchanged.

Table 2. Vertical datum values for tidal stations provided by the Canadian Hydrographic Service (CHS) and the US National Oceanic and Atmospheric Administration (NOAA). Latitude and longitude are in degrees and minutes. Mean Higher High Water (MHHW) and Mean Lower Low Water (MLLW) are defined in two ways: (1) in Canada using tidal predictions derived from tide gauge records; and (2) in the United States using observations from USA tide gauges. All values are referenced to Mean Sea Level (MSL), which by definition in this study is then zero (0.0). Here, CGVD 2013 denotes the Canadian Geodetic Vertical Datum.

Tide gauge ID	Name	Latitude (°N)		Longitude (°W)		CGVD 2013	MSL	MHHW	MLLW
		Deg	Min	Deg	Min	(m)	(m)	(m)	(m)
7795	Point Atkinson	49	20.25	123	22.42	-0.193	0.0	1.30	-1.94
7735	Vancouver	49	17.23	123	6.587	-0.18	0.0	1.32	-1.96
9449424	Cherry Point	48	51.8	122	45.5	-	0.0	1.18	-1.61

2.5. THE SOURCE DISTRIBUTION

Numerical simulation of the 1964 tsunami is based on the revised (Suleimani et al., 2013) coseismic slip distribution for the 1964 rupture based on the model of Suito and Freymueller (2009). This is a three-dimensional viscoelastic model, in combination with an after-slip model, which uses realistic geometry with a shallow-dipping elastic slab to describe the post-seismic deformation that followed the 1964 earthquake. The authors applied the inversion-based model by Johnson et al. (1996) as a basis for their coseismic slip model, adjusting it to the new geometry and critically reinterpreting the coseismic data. Suleimani (2011) used results of the near-field modelling of the 1964 tsunami to constrain the amount of slip placed on intraplate splay faults, and to evaluate the extent of the Patton Bay fault. The revised model includes contributions from coseismic horizontal displacements into the initial tsunami wave field through the component of the ocean surface uplift due to horizontal motion of the steep ocean bottom slopes and was detailed described in the recent paper (Suleimani and Freymueller, 2020). The tsunami simulations revealed that including deformation due to horizontal displacements in the source function resulted in an increase in the far-field tsunami amplitudes. The coseismic vertical deformation resulting is shown in Figure 13.

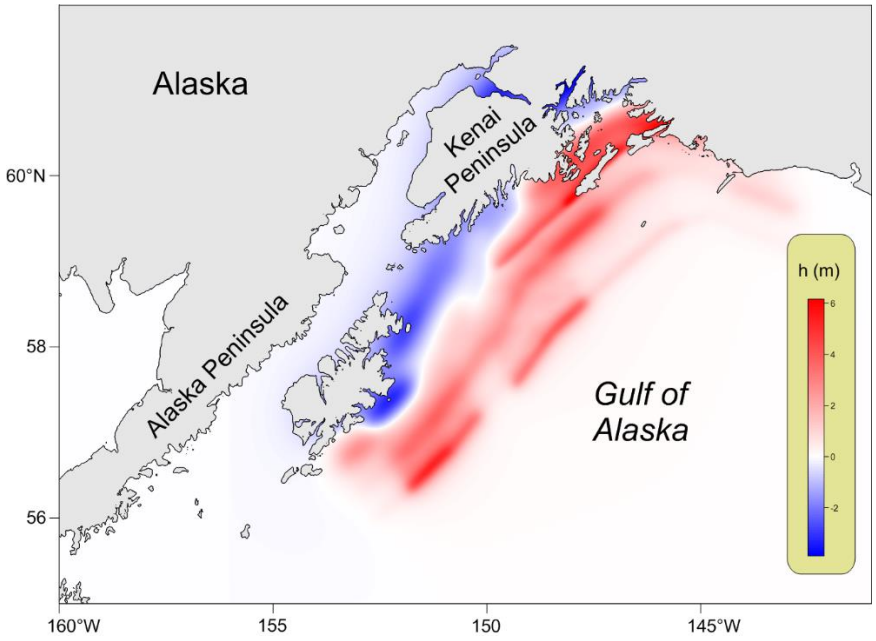

Figure 13. Seafloor vertical displacements (m) at the source region for the March 1964 Alaska tsunami from (Suleimani and Freymueller, 2020). Seafloor displacements, *h*, range from roughly -3 m (blue) to +6 m (red).

3. RESULTS

3.1. MAXIMUM TSUNAMI WAVE HEIGHTS FOR THE COARSE AND INTERMEDIATE GRIDS

The computed distributions of wave height maxima for a future Alaska-type tsunami based on grids 1-3 are presented in Figures 14-18. Figure 14 shows the "rays" of maximum tsunami wave heights for the entire northeast Pacific. While tsunami wave-height maxima are found in Prince Williams Sound (the source area), considerable tsunami energy is radiated to the southeast toward the coast of California. In British Columbia and along the US West Coast, the most affected coastal zones are those exposed to the open ocean, such as the west coast of Vancouver Island and the west coast of Washington State. In more protected areas, such as Juan de Fuca Strait, the computed tsunami wave amplitudes are markedly smaller (Figure 15; Grid 2). The results for Grid 2 are similar for all three sea level rise scenarios

Results for the finer resolution grids (Grids 3) demonstrate the considerable spatial variability in the incoming tsunami wave heights for the study region. Figure 16 shows the distribution of the tsunami wave heights for Grid 3 in the southern Strait of Georgia off Metro Vancouver for the 0.5 m

sea level rise scenario (S1). As the figure indicates, wave amplitudes are much higher in Boundary Bay than near Vancouver to the north. Waves increase toward the shoreline and are especially high in the upper part of Boundary Bay and in Drayton Harbor (see Figure 4 for the location). The pronounced increase in tsunami wave heights in the harbour is related to resonance amplification of the incoming tsunami waves.

For scenarios S2 and S3, corresponding to 1 m and 2 m global sea level rises, respectively, the amplitudes of the waves are generally smaller than amplitudes for Scenario-S1. The decrease in tsunami amplitudes for the higher sea level rise is due to an increase in flooding in the lowlands in the Greater Vancouver region, which, in turn, is not related to inundation by the tsunami waves but to the initial condition (see Figures 6 and 7). The effect of the initial flooding of the low laying area in Boundary Bay was corrected for the final grid (see next section).

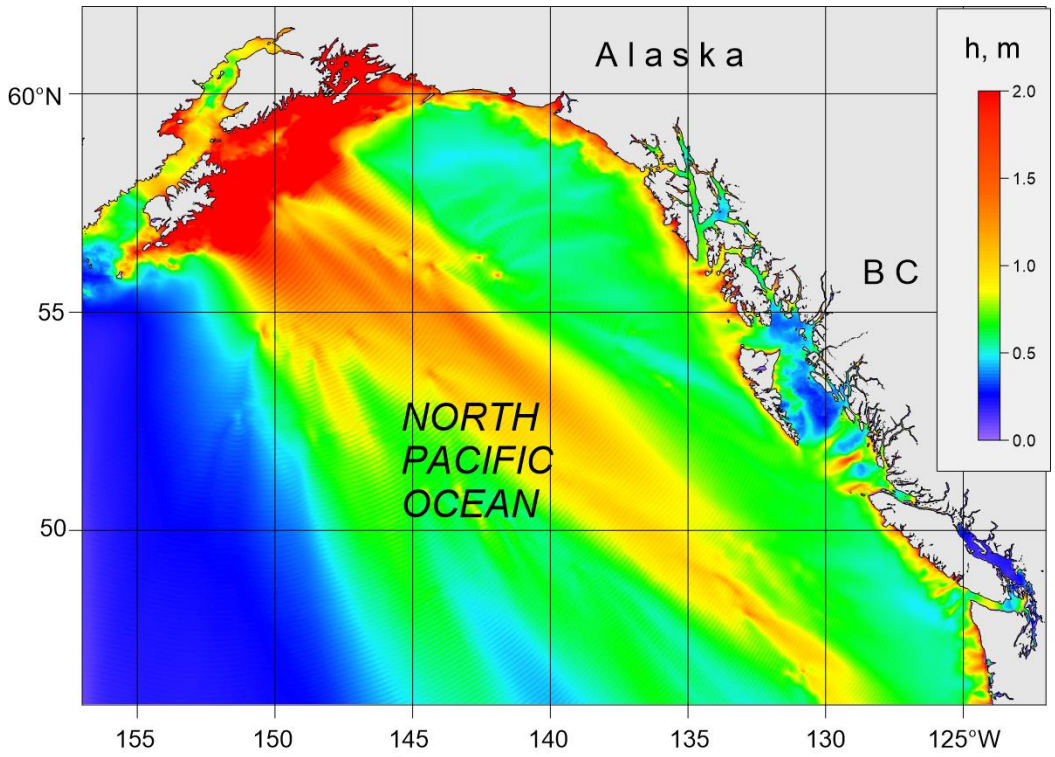

Figure 14. Distribution of maximum tsunami wave heights (metres) for Grid 1 of the nested-grid model for waves generated by simulation of the 1964 tsunami.

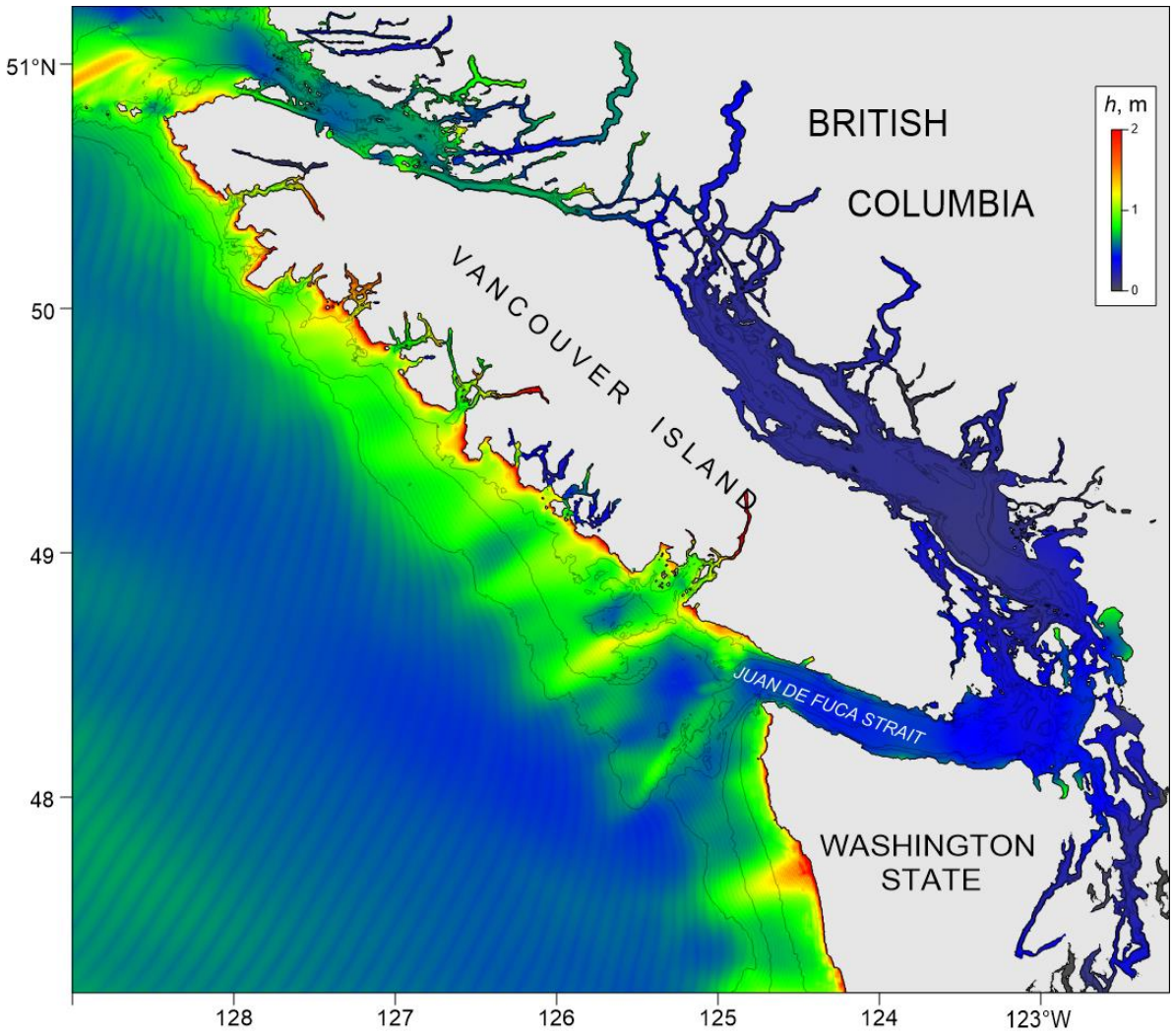

Figure 15. Distribution of maximum tsunami wave heights (metres) for Grid 2 of the nested-grid model for waves generated by simulation of the 1964 tsunami with sea level rise for Scenario-3 (a global 2 m rise by 2200).

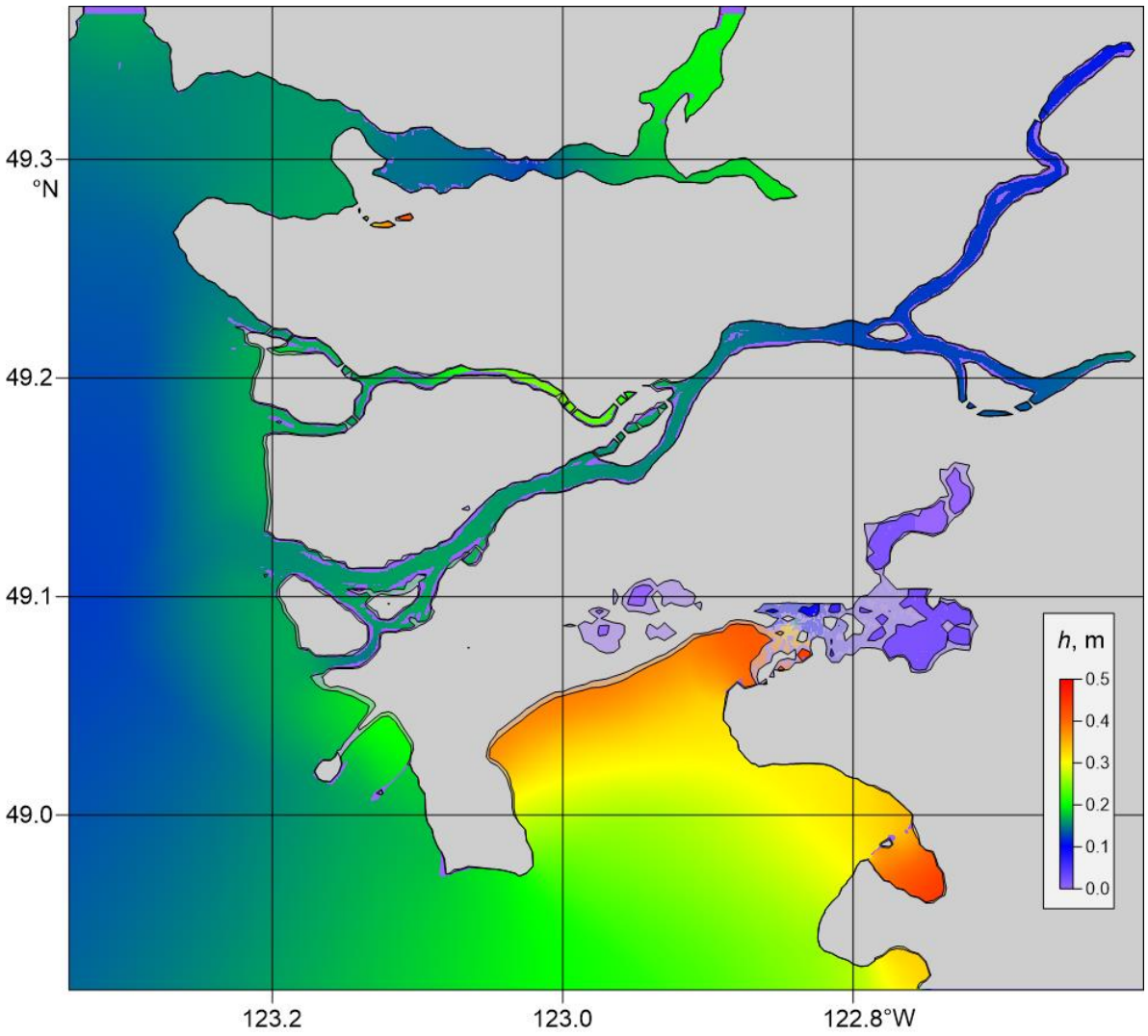

Figure 16. Distribution of maximum tsunami wave heights (metres) for Grid 3 of the nested-grid model for waves generated by simulation of the 1964 tsunami for Scenario-1 (a global sea level rise of 0.5 m).

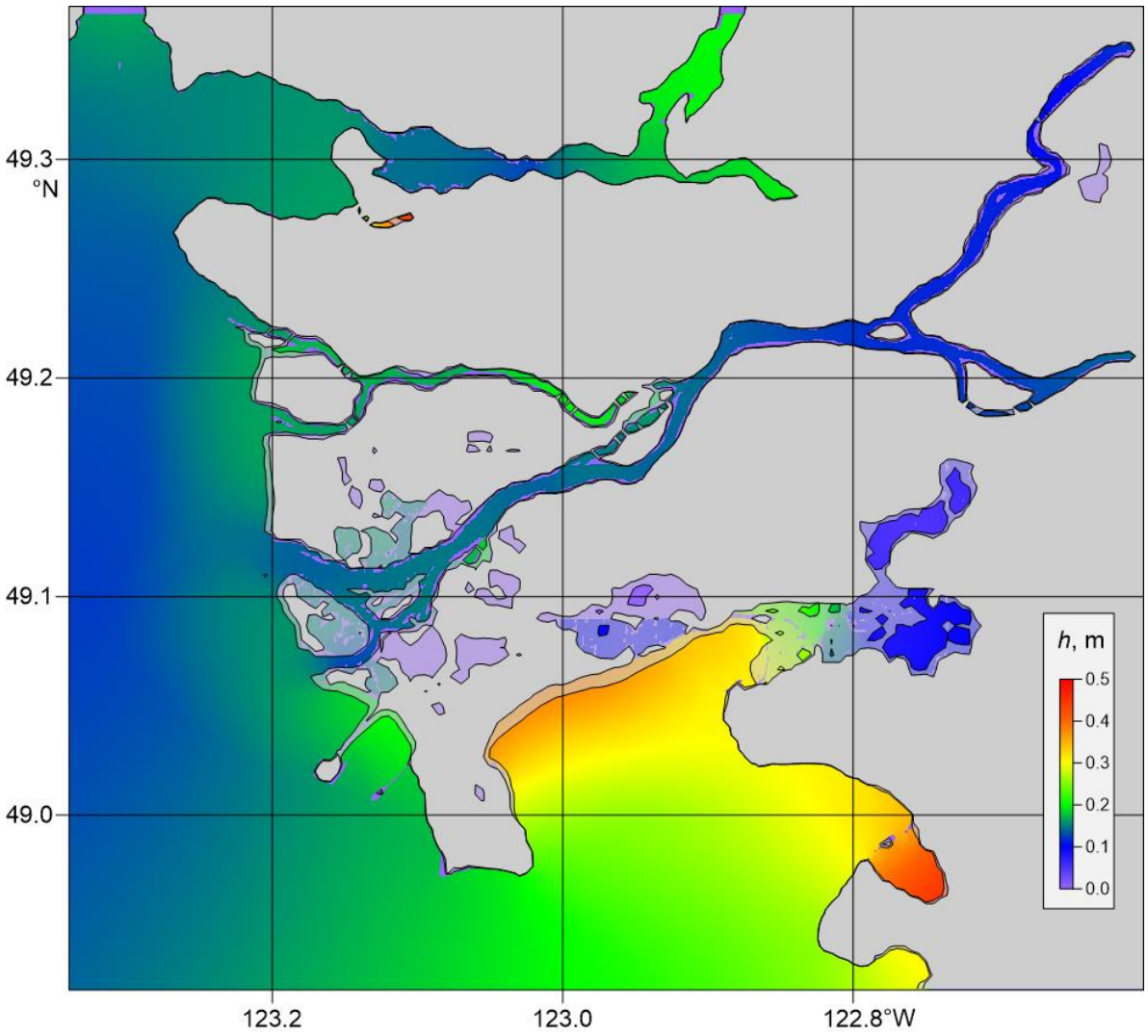

Figure 17. Distribution of maximum tsunami wave heights (metres) for Grid 3 of the nested-grid model for waves generated by simulation of the 1964 tsunami for Scenario-2 (global sea level rise of 1 m).

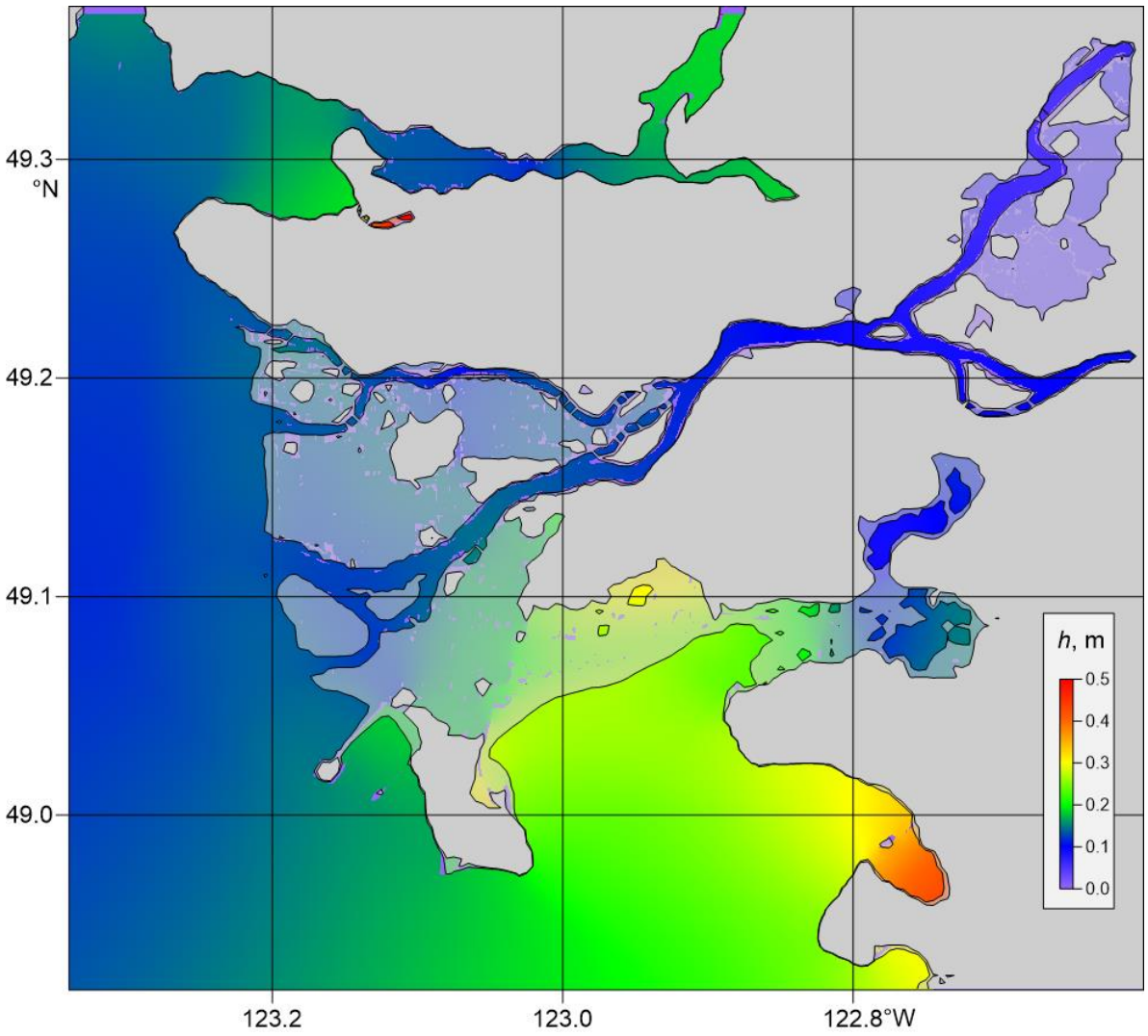

Figure 18. Distribution of maximum tsunami wave heights (metres) for Grid 3 of the nested-grid model for waves generated by simulation of the 1964 tsunami for Scenario-3 (global sea level rise of 2 m).

3.2. DETAILED RESULTS FOR BOUNDARY BAY: TSUNAMI WAVE HEIGHTS AND CURRENTS FOR DIFFERENT SEA LEVEL RISE SCENARIOS.

3.2.1. Wave heights

The tsunami waves for all three sea level rise scenarios were computed using the modified dikes along the northern and eastern sides of Boundary Bay (Grid 4 domain), modifications which negate the possibility of any spill of water from outside the region at the time of the initial conditions. In addition, we prohibited water from entering through the northwestern part of Grid 4 by requiring that other low-laying areas of Greater Vancouver were also protected (numerically at least) from the rising sea.

Figure 19 presents a high-resolution map showing the distribution of the maximum tsunami heights in Boundary Bay and vicinity for Scenario-3 (global sea level rise of 2.0 m). Other scenarios results are generally similar. We note that the amplitudes of the tsunami waves gradually increase from the entrance to the head of the bay and become almost twice as high as those at the entrance (from ~0.25 m to 0.4 m). Another "hot spot" is Drayton Harbor, located at the south-east end of the grid, where waves will reach 0.45 m. Detailed distributions of tsunami heights for all three sea level scenarios are provided for specific areas: (A) Mud Bay (northeastern part of Boundary Bay, Figure 20); (B) The Semiahmoo area (Figure 21); and (C) Drayton Harbor (Figure 22). The locations of the areas A, B, and C are shown in Figure 19.

The highest tsunami waves occur in Mud Bay (Figure 20). The increase in the initial sea level by approximately 0.5 m between Scenarios 1 to 2 increases the tsunami amplitudes by 5% in Mud Bay. However, a further increase in global sea level (Scenario-3) leads to a decrease in the tsunami amplitude at the head of Mud Bay because of the spill of excess water into the upper parts of the Nicomekl and Serpentine rivers. Both effects are minor. In essence, the tsunami amplitudes only weakly depend on the initial levels for the different sea level rise scenarios.

In the Semiahmoo region (Figure 21), the increase in global sea level will flood the Campbell River valley and nearby low-lying areas. This flooding is not related to the tsunami waves but to the initial conditions associated with a given sea level scenario. The tsunami amplitudes only weakly depend on the initial sea levels, with the tsunami amplitudes decreasing only slightly with sea level rise. In Drayton Harbor (Figure 22), the tsunami waves reach amplitude of about 0.4 m are nearly uniformly distributed over the harbour, excluding the harbour entrance. The tsunami amplitudes are almost independent of the initial sea level height, even though in Scenario-3 (2.0 m rise in global sea

level rise), Drayton Spit will be covered by water in several places.

Detailed analysis of the sea level variability was carried out for 12 sites around Boundary Bay (Figures 22-25, Tables 3). The amplitudes and the shape of the tsunami records are similar for all scenarios and all sites. It is clear that the biggest difference is for the shallow sites (1-4), where the increase in sea level leads to a lowering of the bottom friction and an accompanying prolongation of the tsunami oscillations.

3.2.2. Current speeds

Figure 26 shows the distribution of the tsunami-induced current maxima derived from the model. In most places, the current is weak and does not exceed 0.3 cm/s. The rise of global sea level will only weakly change the distribution of tsunami-induced currents. In Mud Bay (Figure 27), the currents are weak, except at the mouth of the Nicomekl River and vicinity, where currents can reach 0.8 m/s and some areas are flooded for Scenarios 2 and 3.

Current along the Semiahmoo coast (Figure 28) are generally weak, except for the mouth of Campbell River, where speeds can reach 1 m/s (2 knots). The current at the mouth of Campbell River will be stronger for Scenario-3 compared to Scenarios 2 and 3 because of the enhanced flooding in the river valley. The current at the entrance to Drayton Harbor (Figure 29) will be the strongest and could reach 1.5 m/s (3 knots). Increasing sea level will decrease the current at the harbour mouth because of an increase in water depth.

Details on the behaviour of the tsunami-induced currents for the sites 1-12 are shown in Figures 30-35 and in Table 4. Generally, the current velocity time series are remarkably similar for all three sea level rise scenarios. The strongest currents (up to 0.53 m/s) are at Site 8, located in the eastern sector of Boundary Bay. At other sites, current speeds do not exceed 0.3 m/s.

The tsunami travel time to Boundary Bay from the 1964 Alaska source region is around 5 hours. The initial wave crest reaches the region 6 hours after the earthquake, with the tsunami waves first arriving at Sites 9,10, and 11, located on the Semiahmoo coast, then Sites 8 and 7 and, finally, Site 1, approximately half an hour after reaching the Semiahmoo coast. The first wave is the highest, followed by the second wave, which is only marginally lower. The subsequent waves are lower than the first two waves.

In general, waves from the Alaska 1964 tsunami are relatively small in Boundary Bay and wave parameters do not change very much with sea level rise. However, sea level rise will increase the effect of small tsunamis as tsunami flooding will be superposed on pre-tsunami sea levels. Tsunami generated currents will also not be significantly affected by sea level rise, except in areas like the entrance to Drayton Harbor, where moderate wave-induced currents will occur. Such waves could be a hazard to small boats.

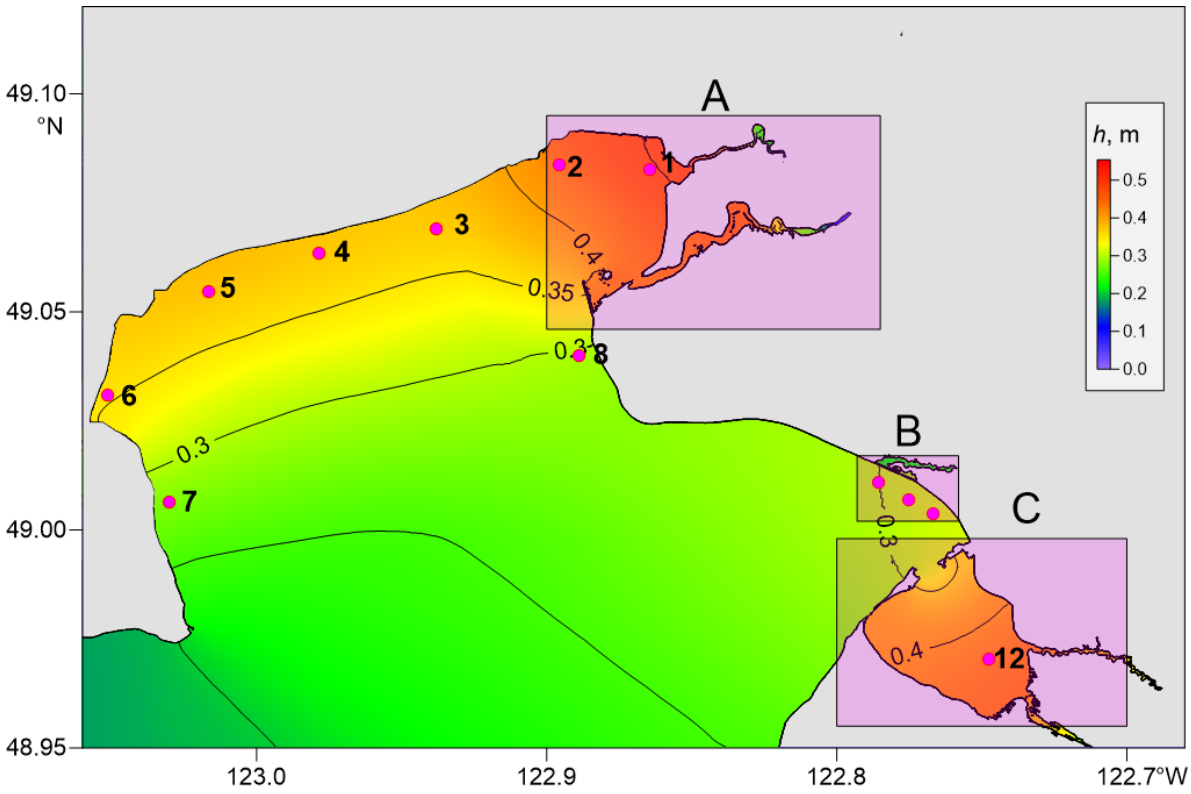

Figure 19. Distribution of maximum tsunami wave heights (metres) for Grid 4 of the nested-grid model for waves generated by simulation of the 1964 tsunami for sea level rise Scenario S3. Numbers in Boundary Bay denote sites for which tsunami wave records have been simulated. Letters A, B and C denote regions shown in greater detail for all three scenarios in Figures 20-22.

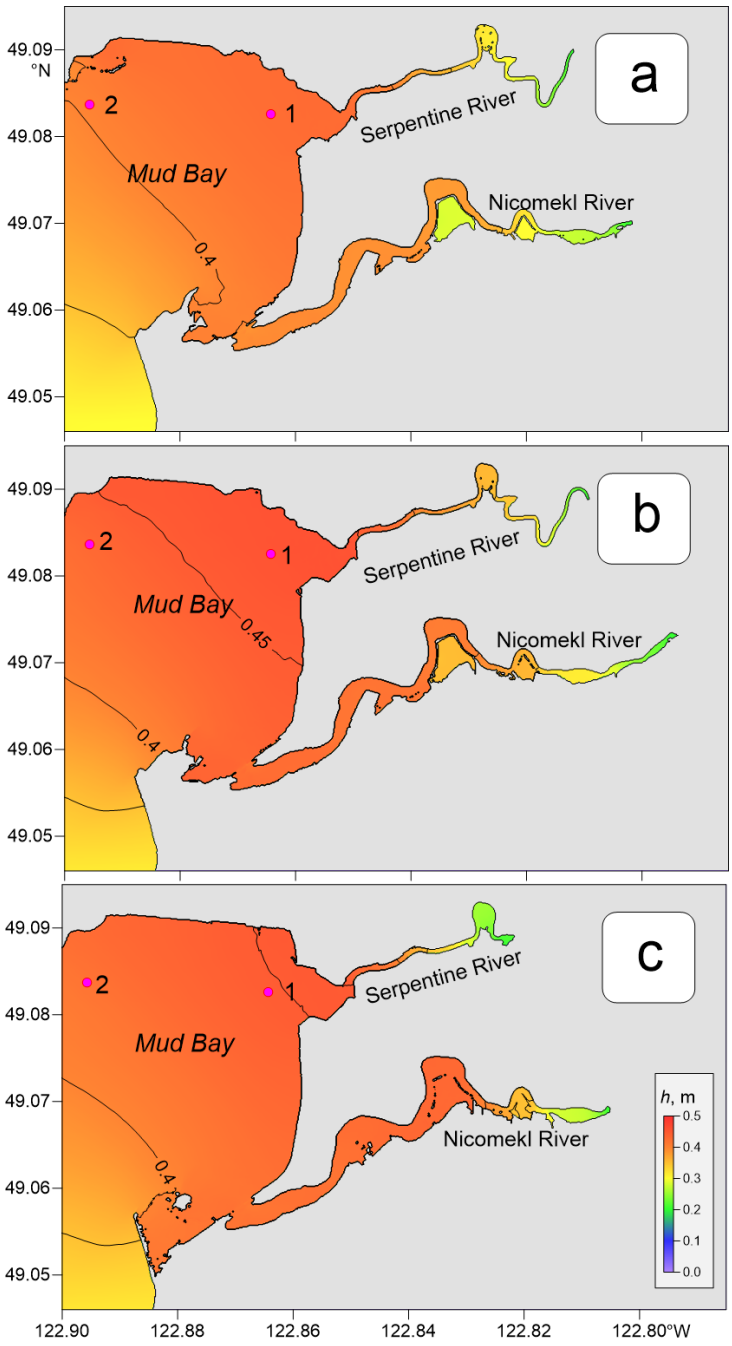

Figure 20. Distribution of maximum tsunami wave heights (metres) for Segment A (Mud Bay, see Figure 19 for the reference) for waves generated by simulation of the 1964 tsunami for sea level rise Scenarios 1-3 (a-c, respectively). Numbers in Boundary Bay denote sites for which tsunami wave records have been simulated.

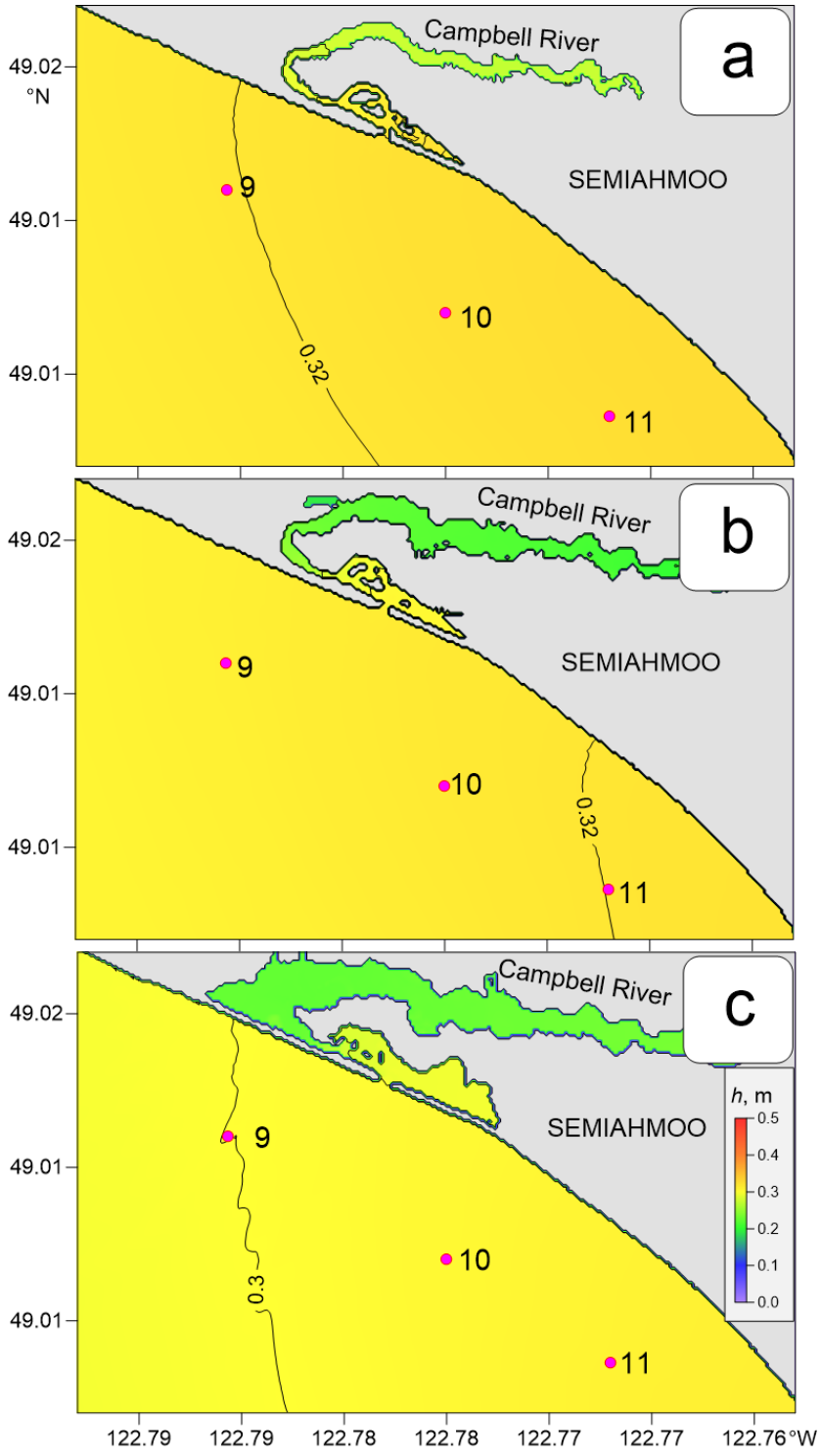

Figure 21. Distribution of maximum tsunami wave heights (metres) for Segment B (Semiahmoo, see Figure 19 for the reference) for waves generated by simulation of the 1964 tsunami for sea level rise Scenarios 1-3 (a, b and c, respectively). Numbers in Boundary Bay denote sites for which tsunami wave records have been simulated.

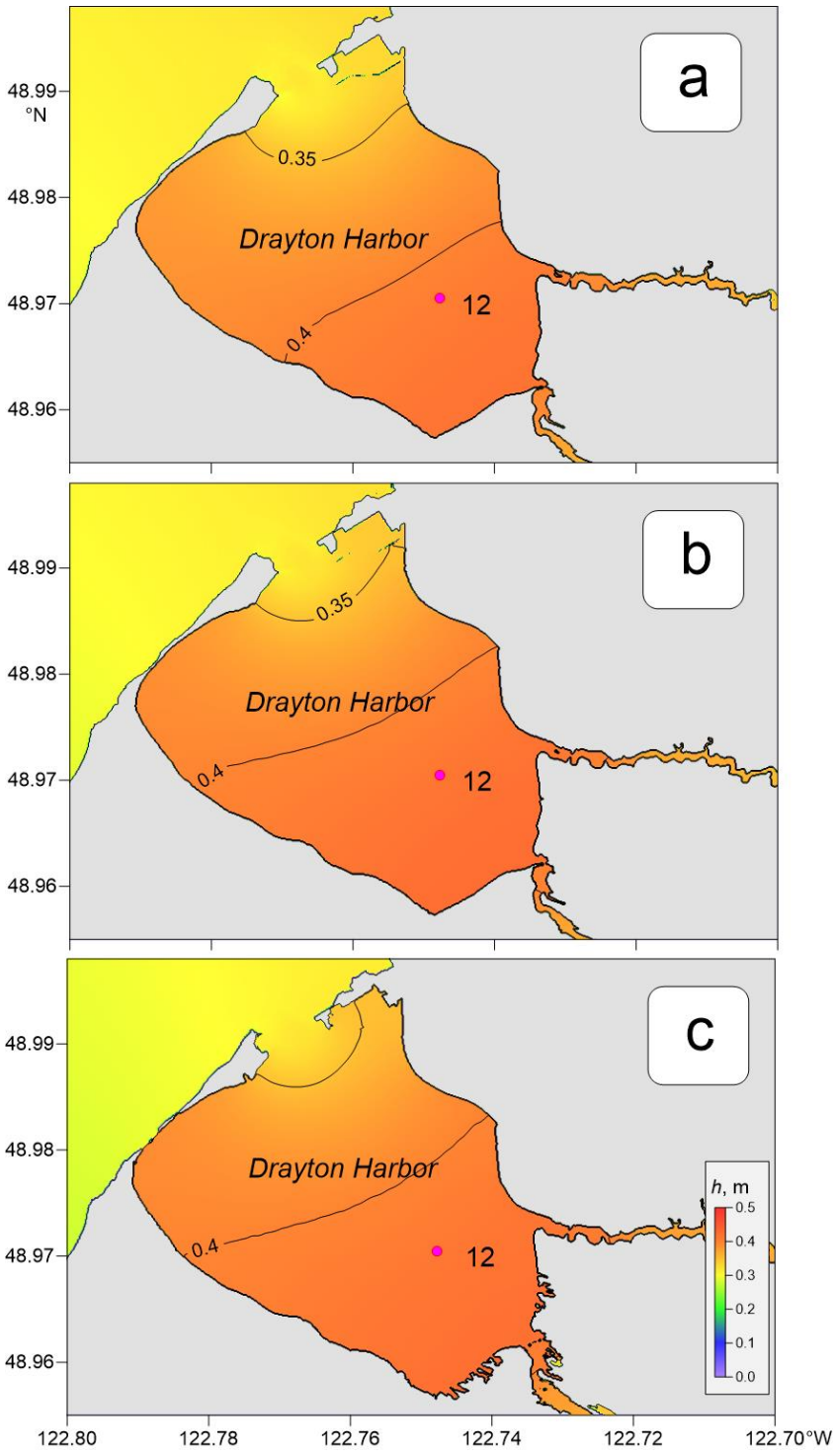

Figure 22. Distribution of maximum tsunami wave heights (metres) for Segment C (Drayton Harbor, see Figure 19 for the reference) for waves generated by simulation of the 1964 tsunami for sea level rise Scenarios 1-3 (a, b and c, respectively). Numbers in Boundary Bay denote sites for which tsunami wave records have been simulated.

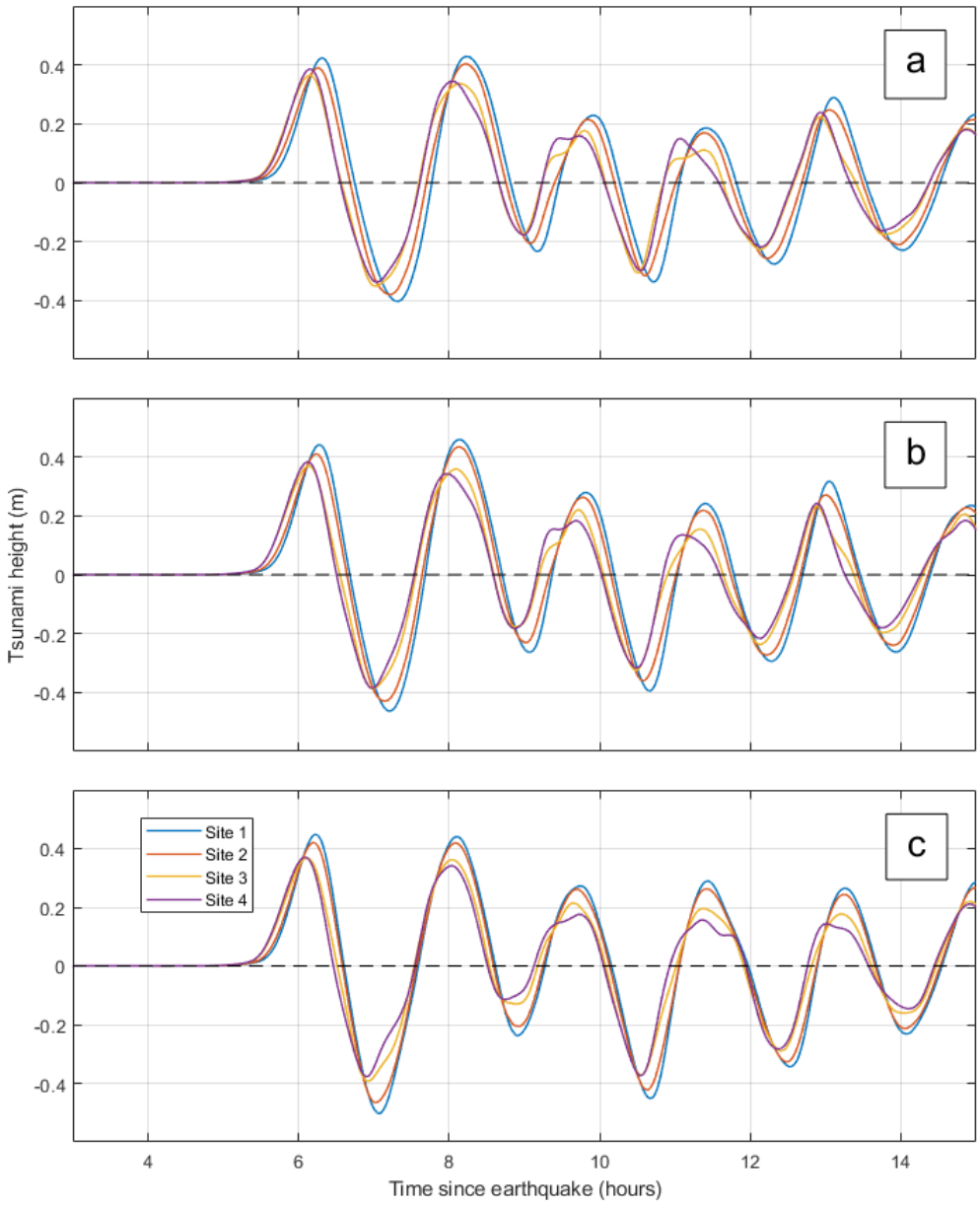

Figure 23. Simulated records of sea level variation for the Alaska 1964-type tsunami at sites 1 – 4 for sea level rise: (a) Scenario-1 (0.5 m global sea level rise case); (b) Scenario-2 (1 m global sea level rise case); and (c) Scenario-3 (2 m global sea level rise case). See Figure 19 for the site locations.

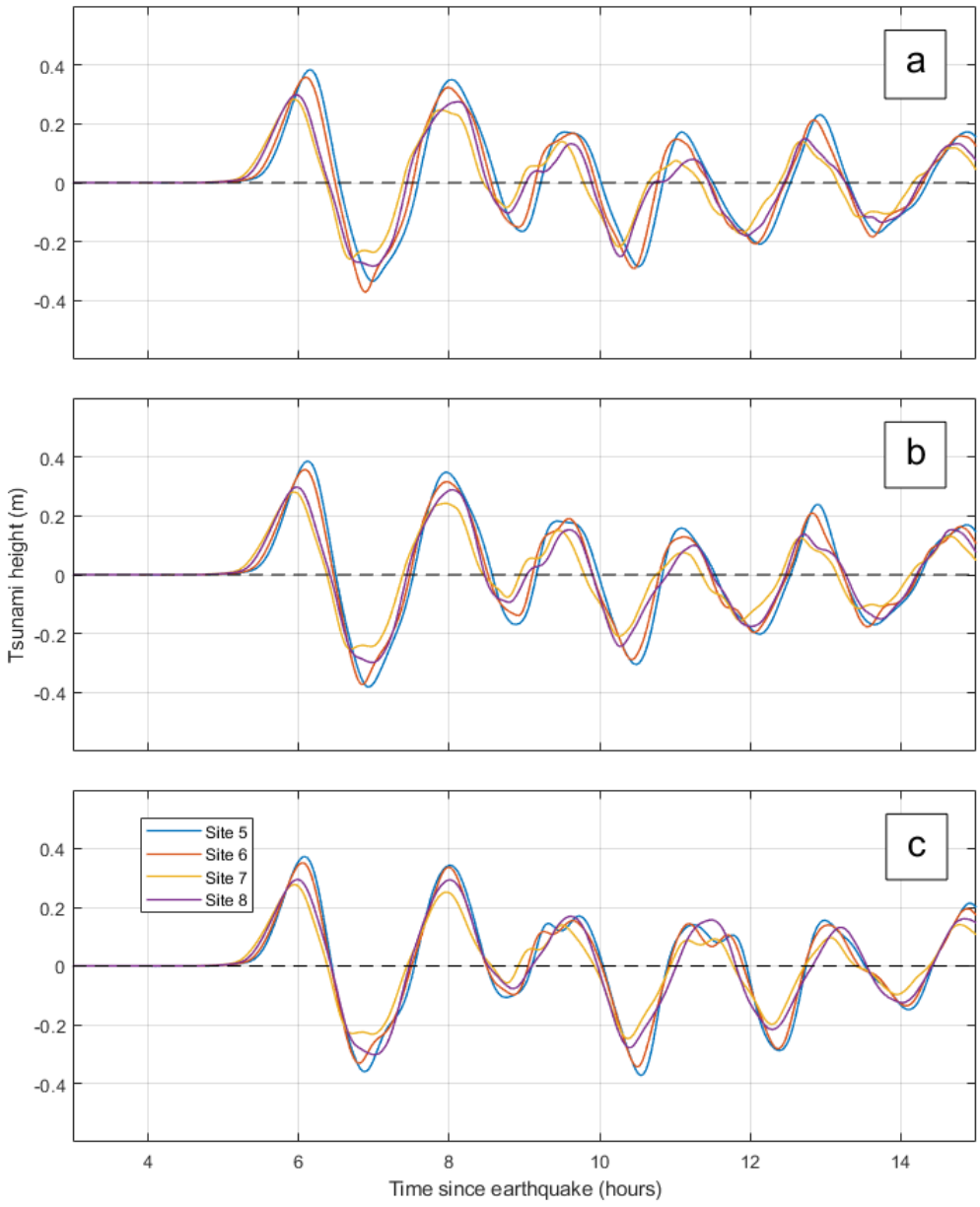

Figure 24. Simulated records of sea level variation for the Alaska 1964-type tsunami at sites 5 – 8 for sea level rise: (a) Scenario-1 (0.5 m global sea level rise case); (b) Scenario-2 (1 m global sea level rise case); and (c) Scenario-3 (2 m global sea level rise case). See Figure 19 for the site locations.

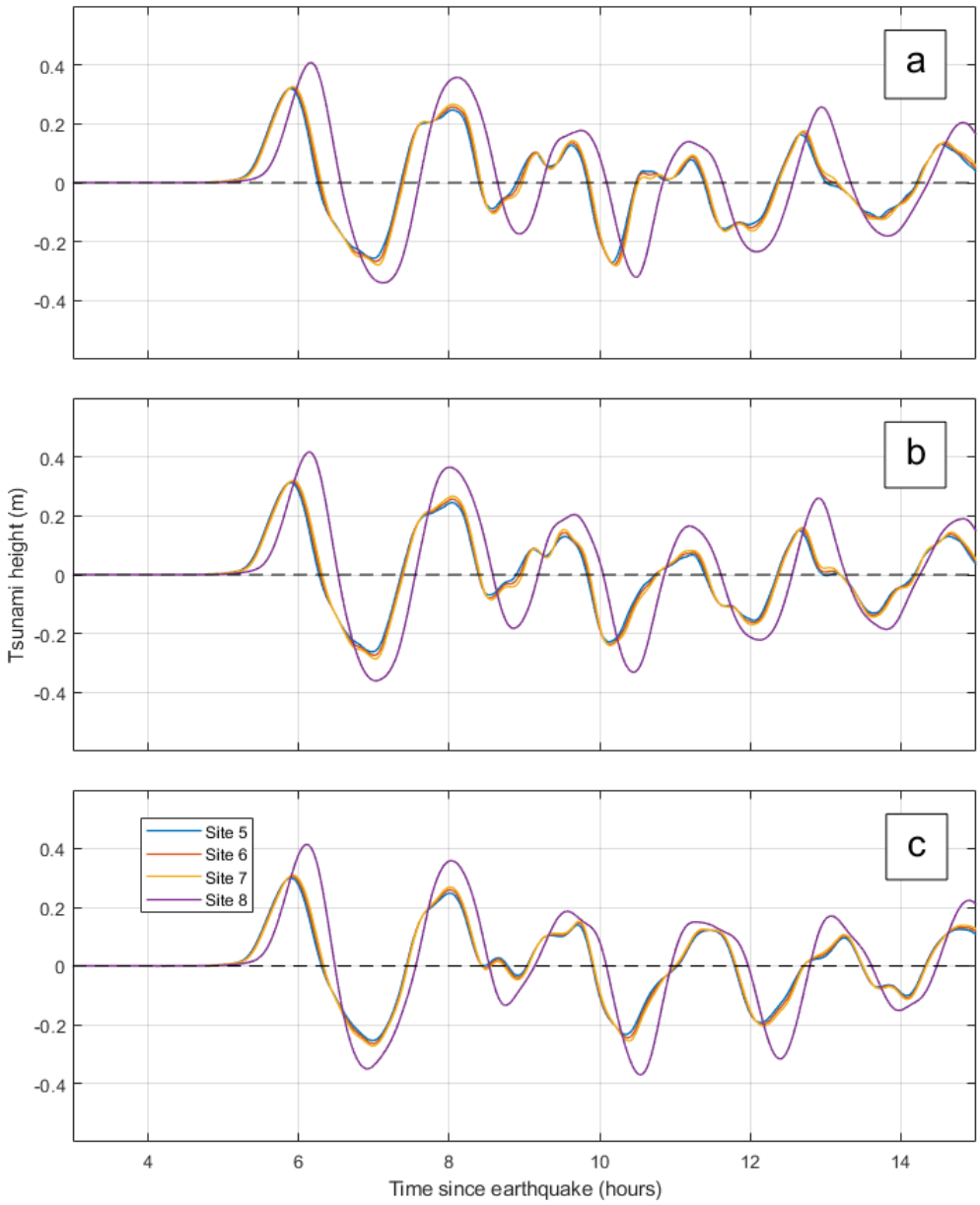

Figure 25. Simulated records of sea level variation for the Alaska 1964-type tsunami at sites 9 – 12 (a): Scenario-1 (0.5 m global sea level rise case); (b) Scenario-2 (1 m global sea level rise case); and (c) Scenario-3 (2 m global sea level rise case). See Figure 19 for the site locations.

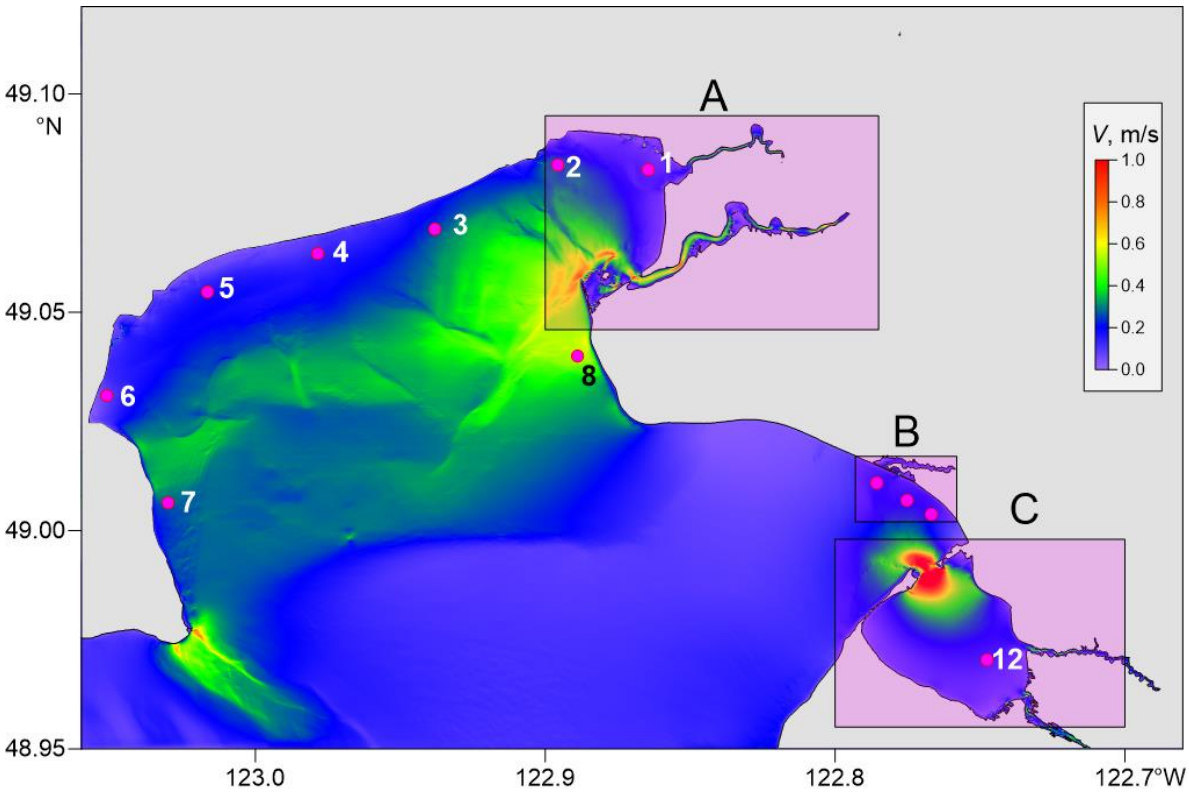

Figure 26. Distribution of maximum tsunami generated current (m/s) for Grid 4 of the nested-grid model for waves generated by simulation of the 1964 tsunami. Numbers in Boundary Bay denote sites for which tsunami wave records have been simulated.

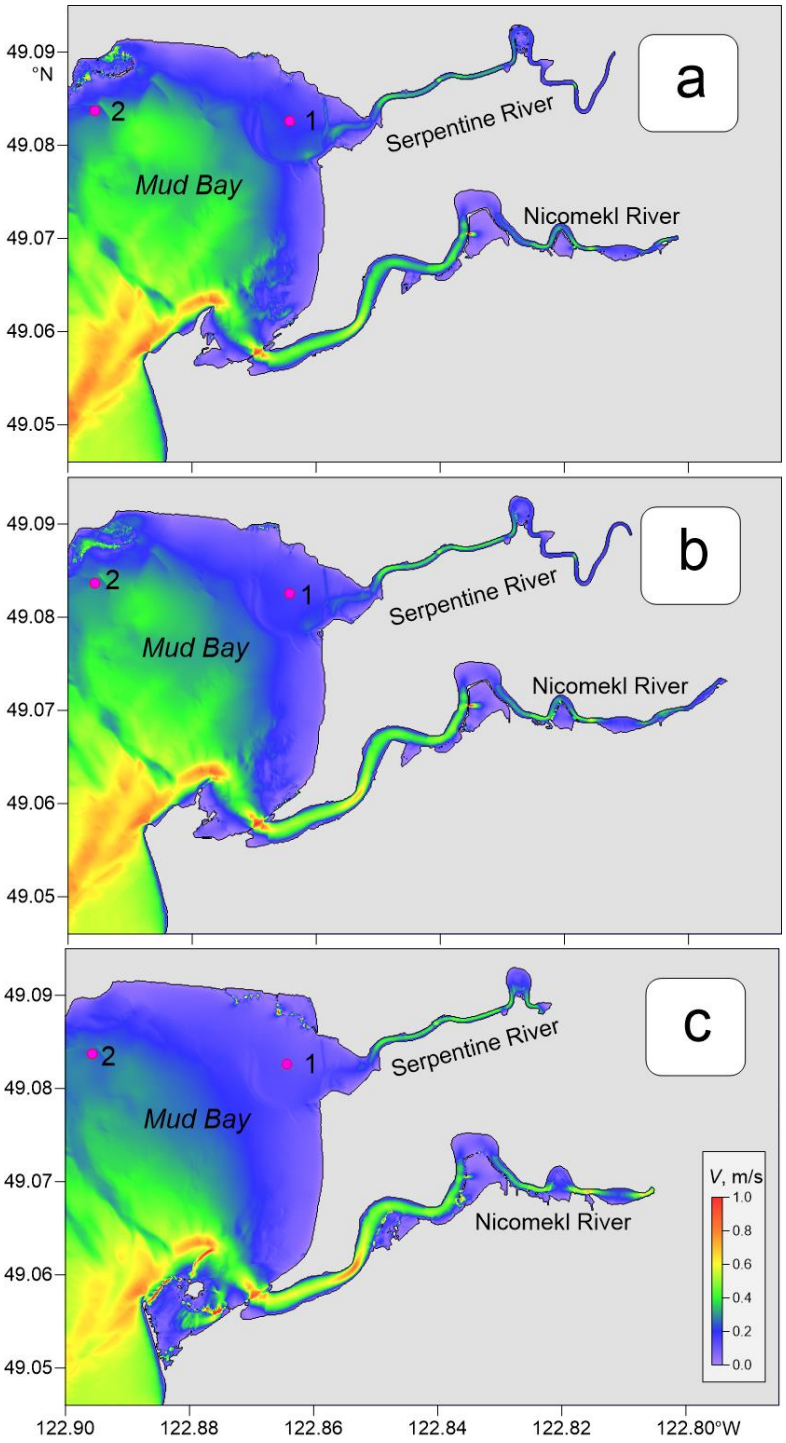

Figure 27. Distribution of maximum tsunami generated currents (m/s) for Segment A (Mud Bay, see Figure 23 for the reference) for waves generated by simulation of the 1964 tsunami for sea level rise Scenarios 1-3 (a, b, and c, respectively). Numbers in Boundary Bay denote sites for which tsunami wave records have been simulated.

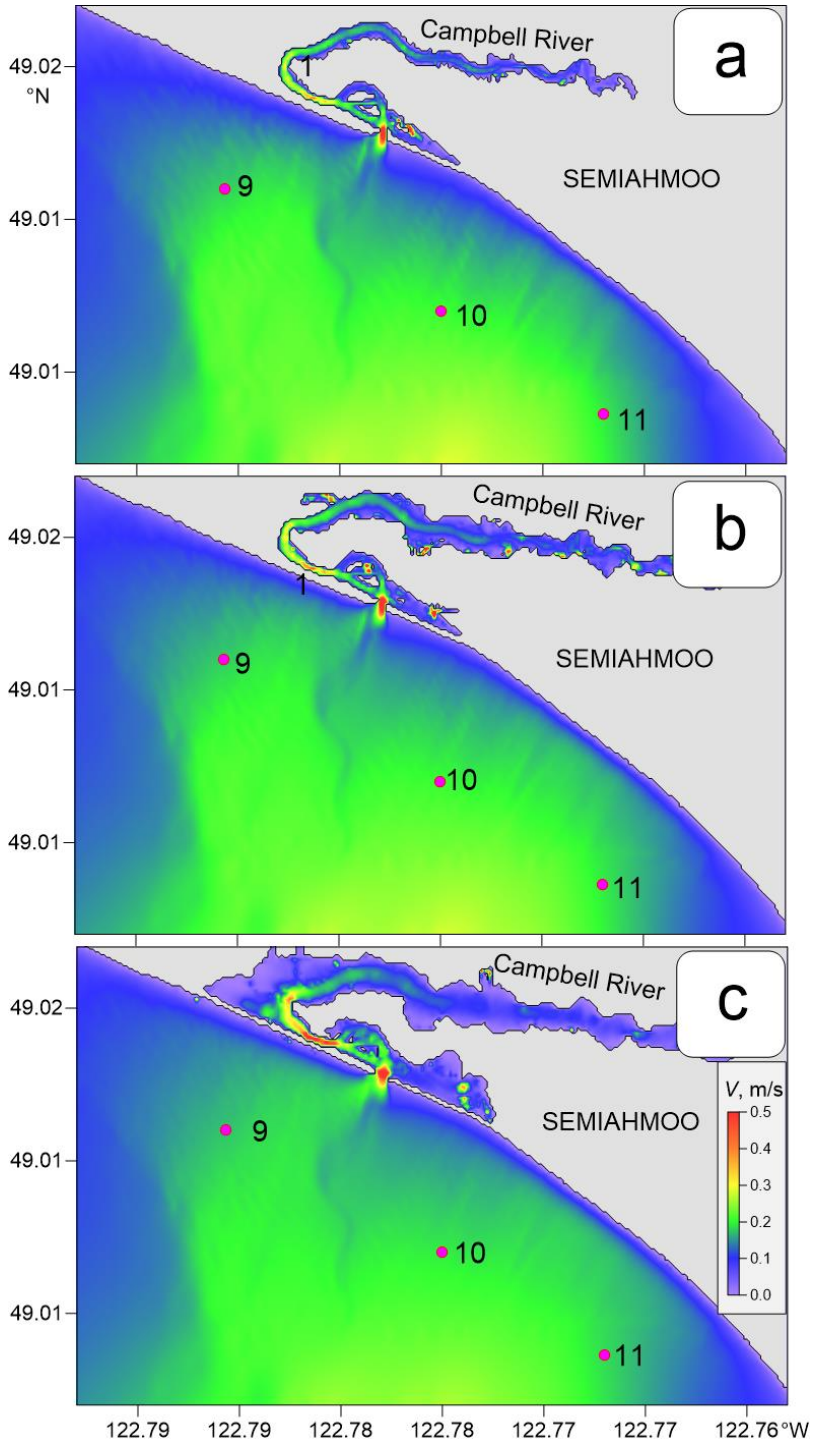

Figure 28. Distribution of maximum tsunami generated currents (m/s) for Segment B (Semiahmoo, see Figure 23 for the reference) for waves generated by simulation of the 1964 tsunami: (a) Scenario-1 (0.5 m global sea level rise case); (b) Scenario-2 (1 m global sea level rise case); and (c) Scenario-3 (2 m global sea level rise case). Numbers in Boundary Bay denote sites for which tsunami wave records have been simulated.

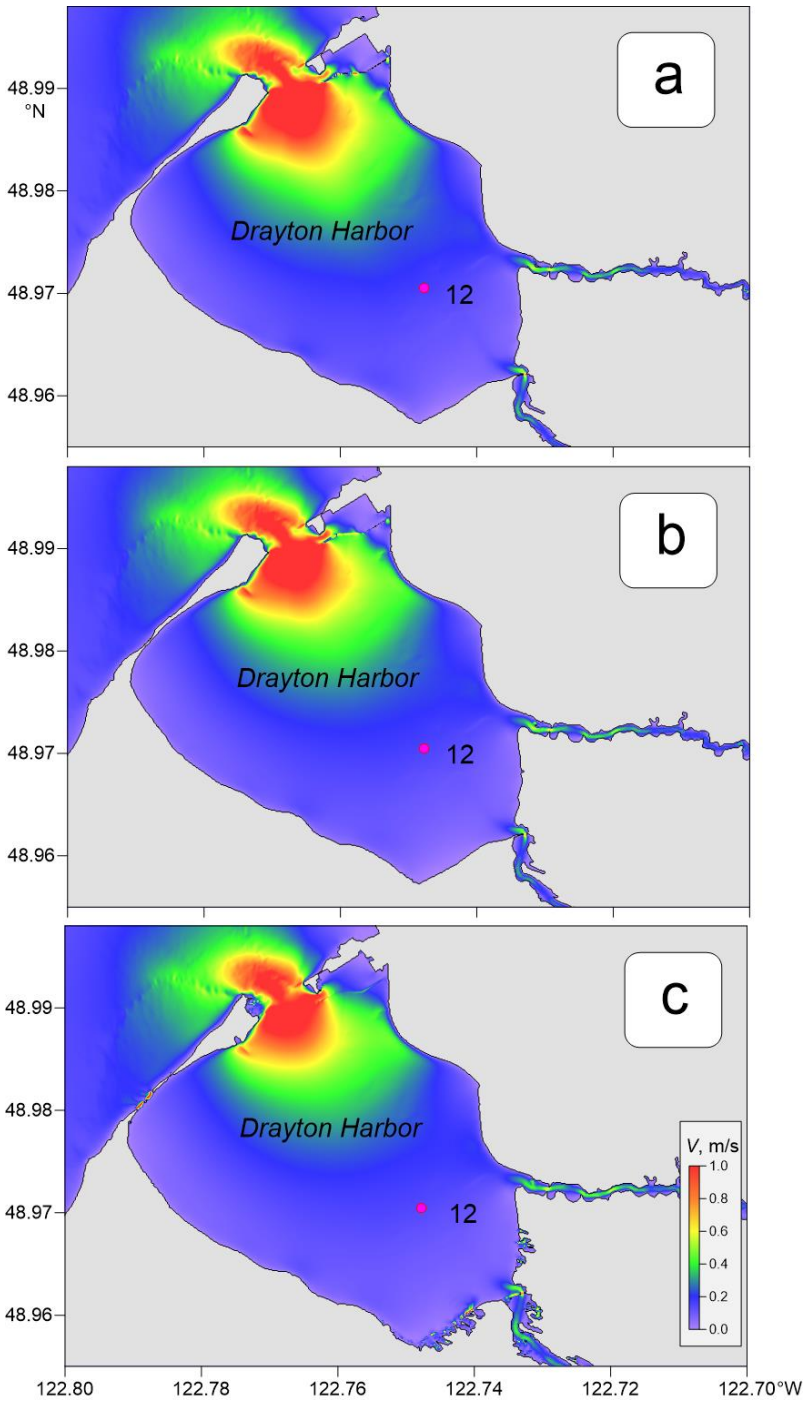

Figure 29. Distribution of maximum tsunami generated currents (m/s) for Segment C (Dayton Harbor, see Figure 23 for the reference) for waves generated by simulation of the 1964 tsunami: (a) Scenario-1 (0.5 m global sea level rise case); (b) Scenario-2 (1 m global sea level rise case); and (c) Scenario-3 (2 m global sea level rise case). Numbers in Boundary Bay denote sites for which tsunami wave records have been simulated.

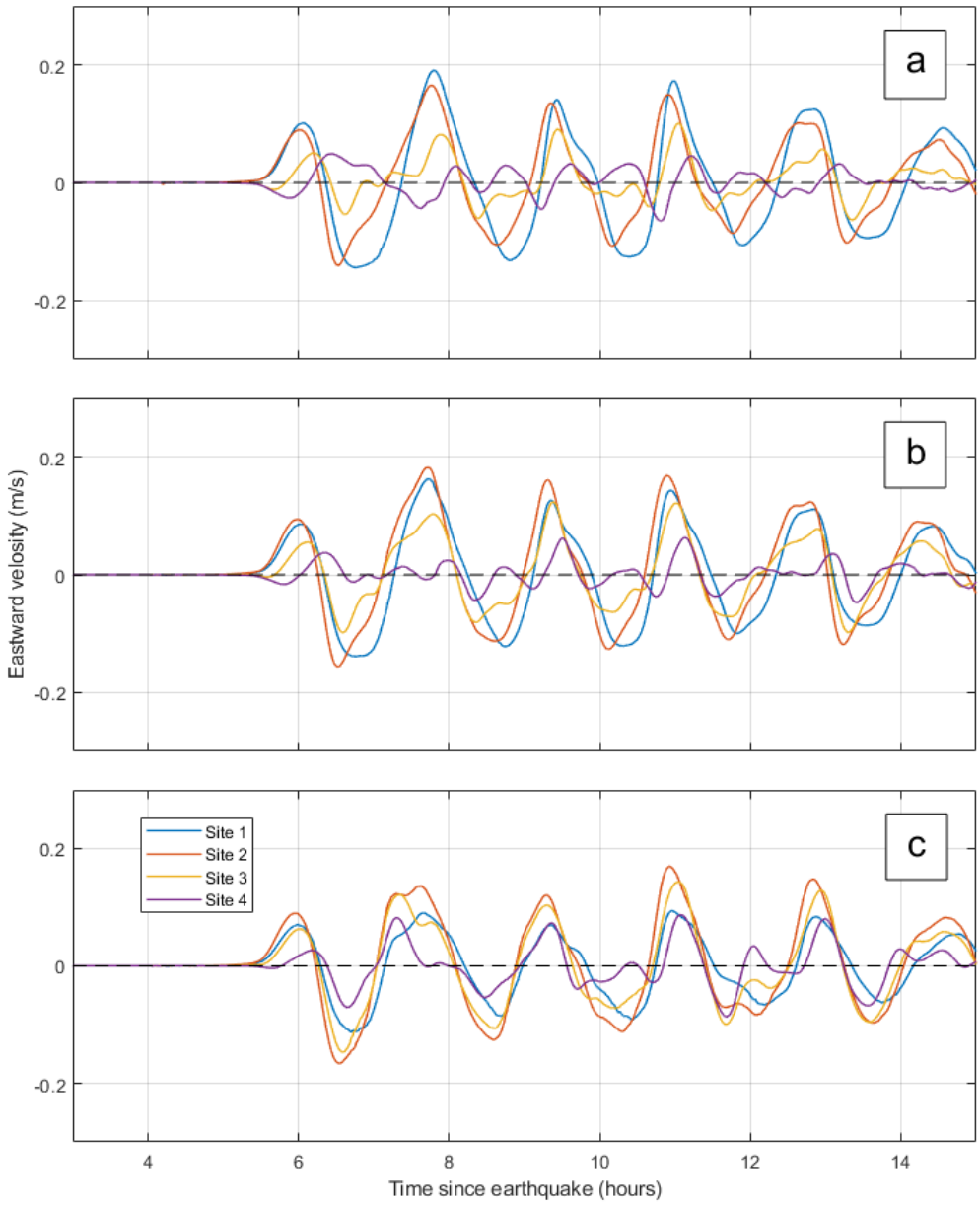

Figure 30. Simulated records of the eastward component of current velocity for the Alaska 1964-type tsunami at sites 1-4: (a) Scenario-1 (0.5 m global sea level rise case); (b) Scenario-2 (1 m global sea level rise case); and (c) Scenario-3 (2 m global sea level rise case). See Figure 26 for the site locations.

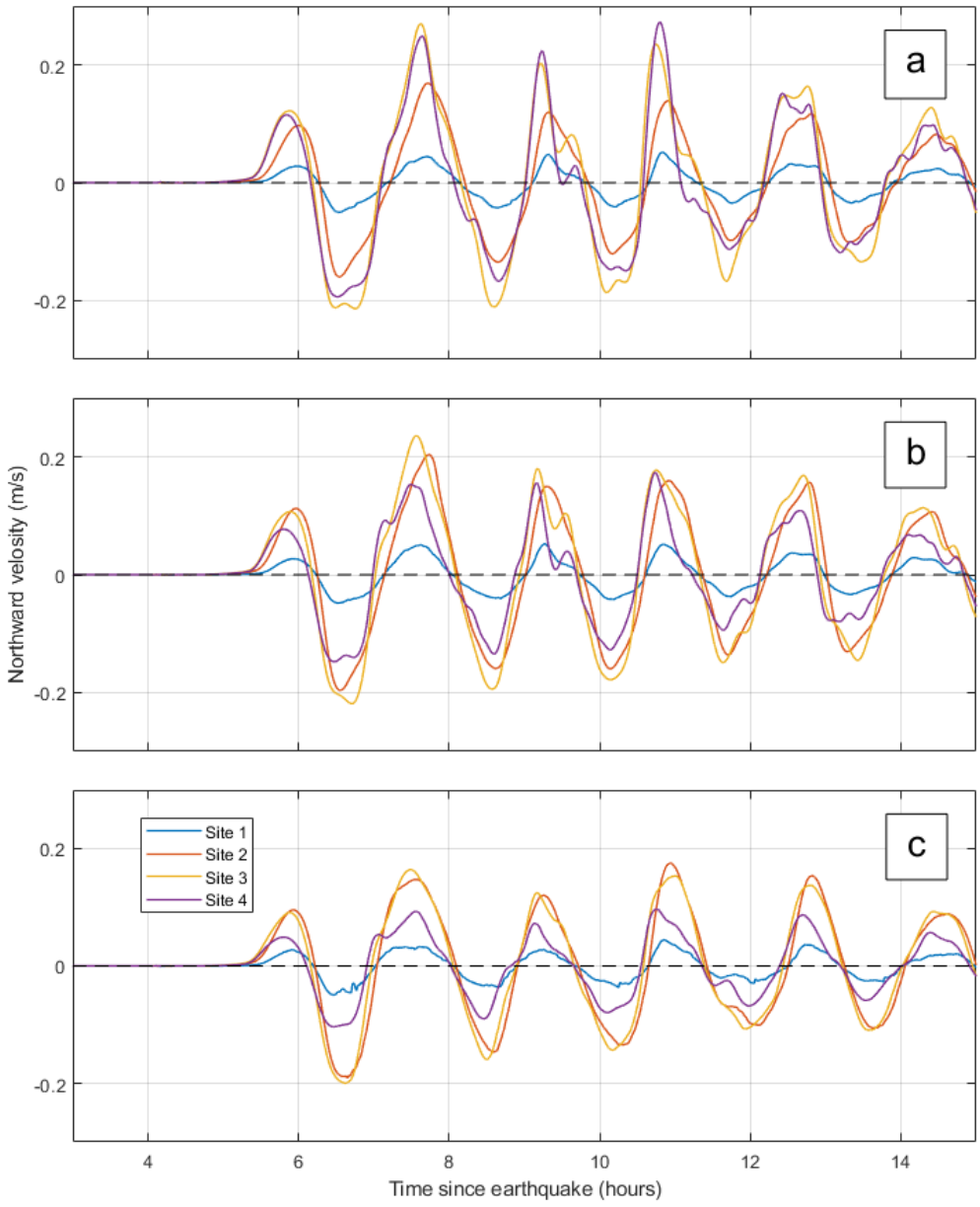

Figure 31. Simulated records of the northward component of current velocity for the Alaska 1964-type tsunami at sites 1-4: (a) Scenario-1 (0.5 m global sea level rise case); (b) Scenario-2 (1 m global sea level rise case); and (c) Scenario-3 (2 m global sea level rise case). See Figure 26 for the site locations.

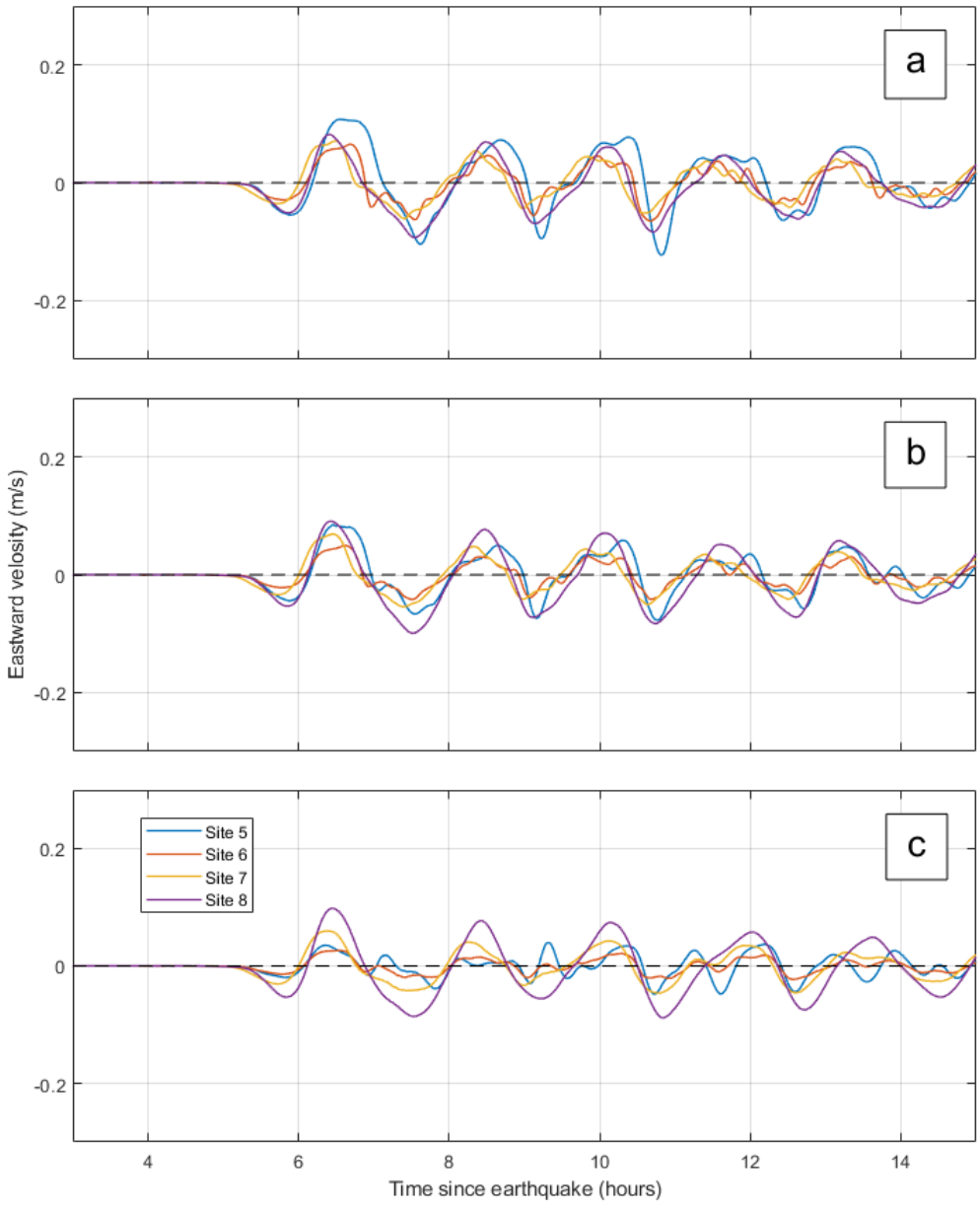

Figure 32. Simulated records of the eastward component of current velocity for the Alaska 1964-type tsunami at sites 5-8: (a) Scenario-1 (0.5 m global sea level rise case); (b) Scenario-2 (1 m global sea level rise case); and (c) Scenario-3 (2 m global sea level rise case). See Figure 26 for the site locations.

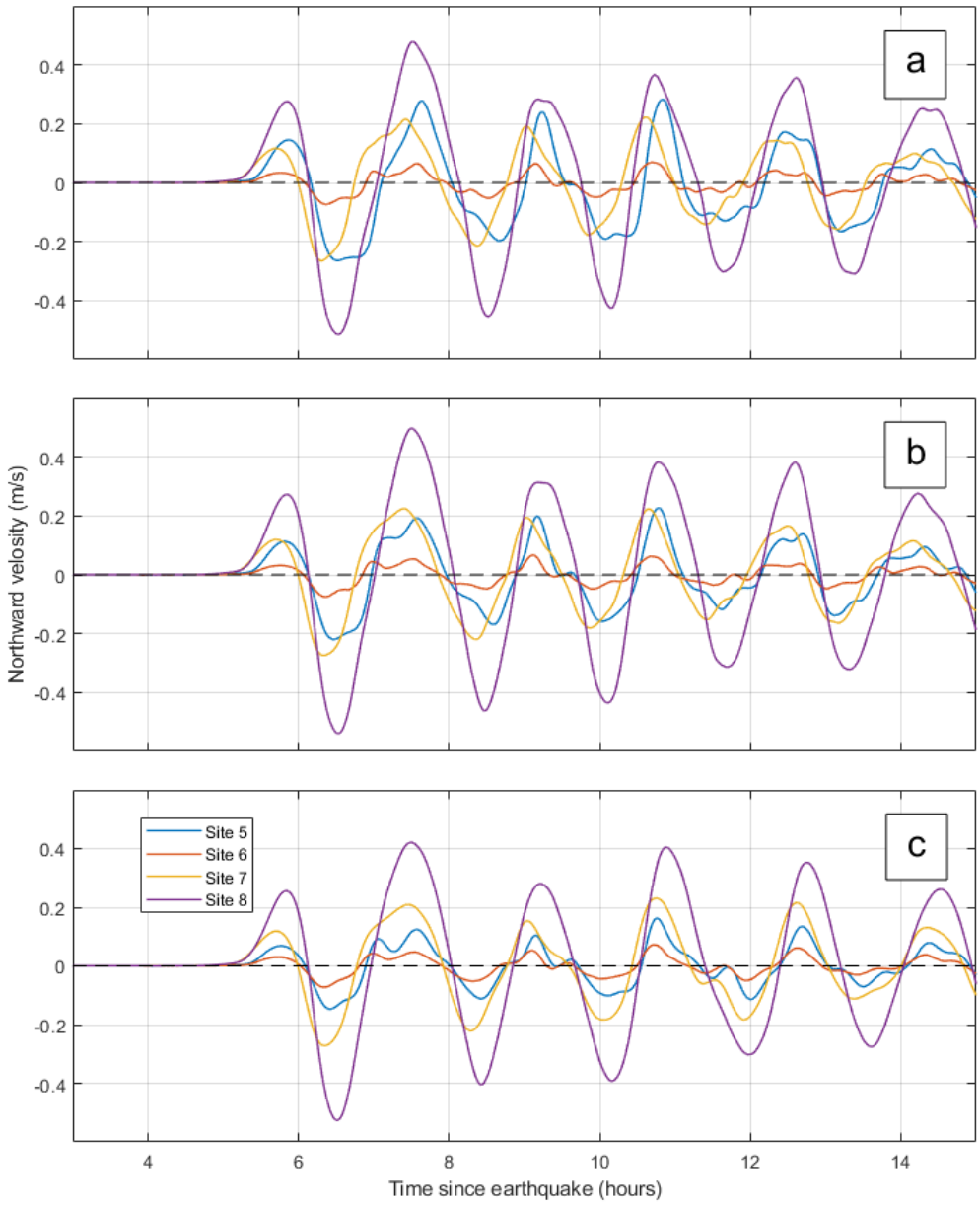

Figure 33. Simulated records of the northward component of current velocity for the Alaska 1964-type tsunami at sites 5-8: (a) Scenario-1 (0.5 m global sea level rise case); (b) Scenario-2 (1 m global sea level rise case); and (c) Scenario-3 (2 m global sea level rise case). See Figure 26 for the site locations.

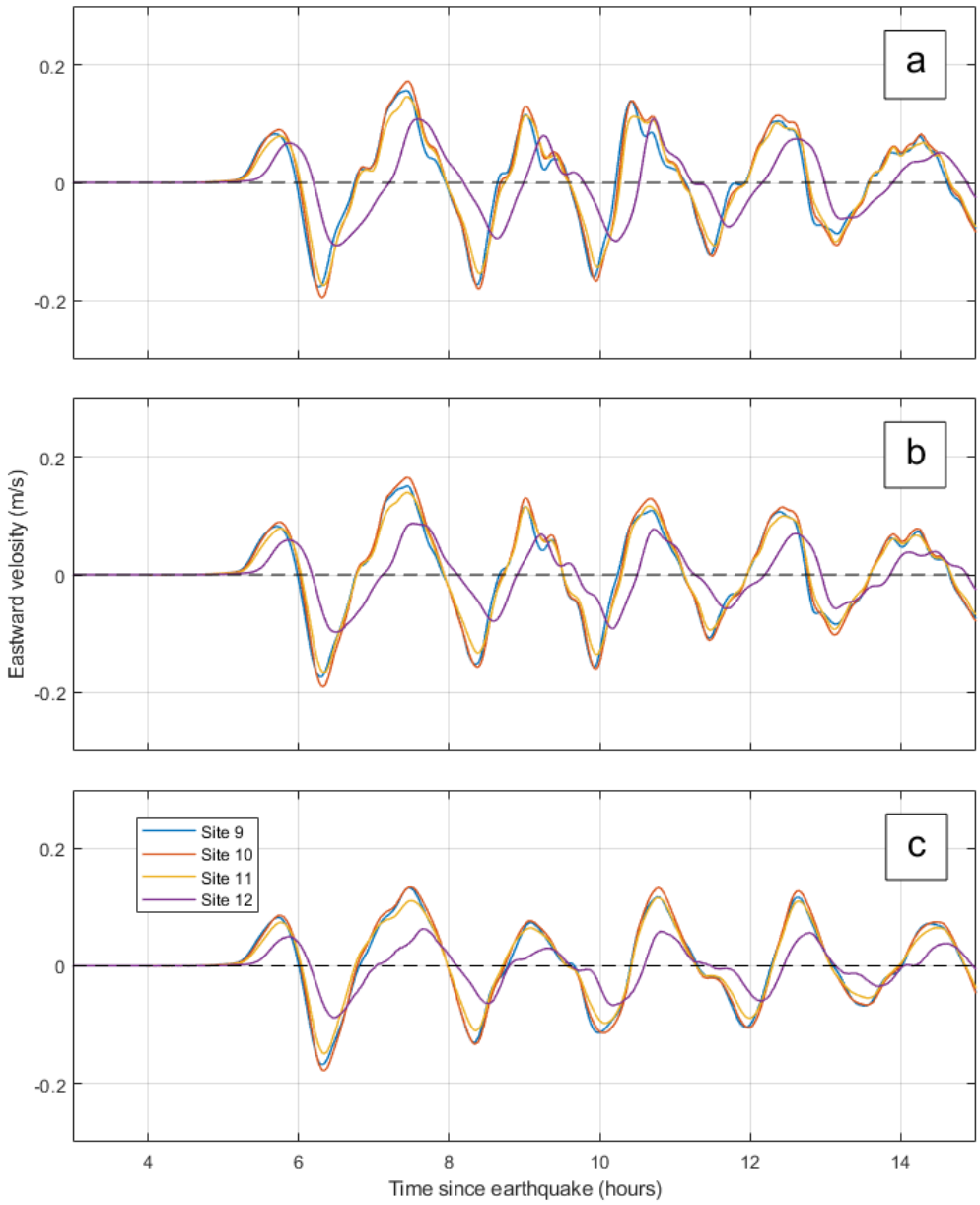

Figure 34. Simulated records of the eastward component of current velocity for the Alaska 1964-type tsunami at sites 9-12: (a) Scenario-1 (0.5 m global sea level rise case); (b) Scenario-2 (1 m global sea level rise case); and (c) Scenario-3 (2 m global sea level rise case). See Figure 26 for the site locations.

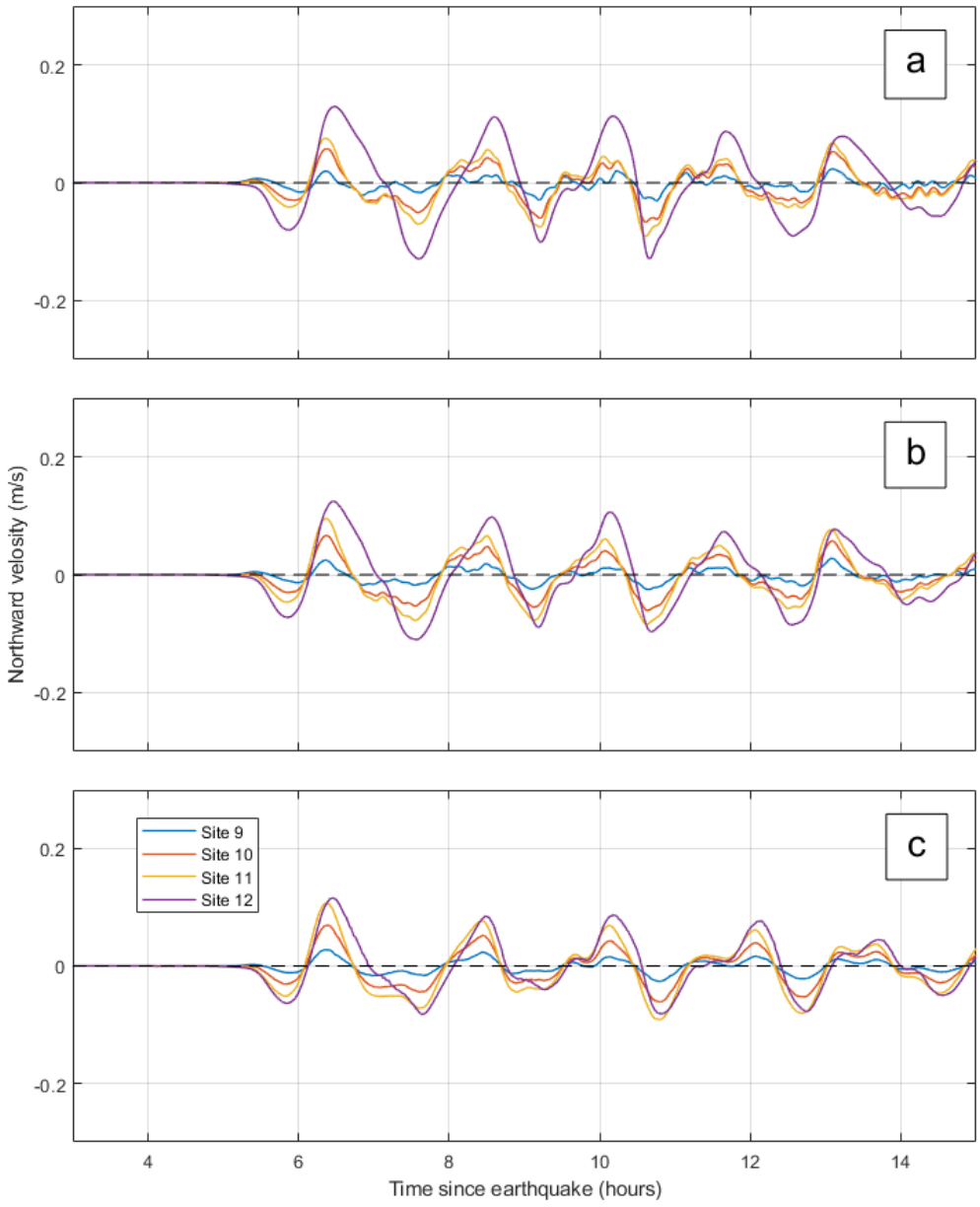

Figure 35. Simulated records of the northward component of current velocity for the Alaska 1964-type tsunami at sites 9-12: (a) Scenario-1 (0.5 m global sea level rise case); (b) Scenario-2 (1 m global sea level rise case); and (c) Scenario-3 (2 m global sea level rise case). See Figure 26 for the site locations.

Table 3. Tsunami wave parameters for the Alaska 1964 tsunami at Boundary Bay for numerical simulations for the three sea level rise scenarios, S1 to S3. See Figures 20-21 for the site locations. Travel times for the maximum waves are in hours and minutes (HH:MM) after the start of the earthquake.

Site No	Highest crest						Deepest trough					
	Height (m)			Travel time HH:MM			Height (m)			Travel time HH:MM		
	S1	S2	S3	S1	S2	S3	S1	S2	S3	S1	S2	S3
1	0.43*	0.46*	0.45	8:14	8:08	6:14	-0.40	-0.46	-0.50	7:19	7:13	7:04
2	0.40*	0.43*	0.42	8:13	8:08	6:13	-0.38	-0.43	-0.47	7:13	7:09	7:01
3	0.37	0.37	0.37	6:09	6:08	6:07	-0.35	-0.39	-0.39	7:01	6:59	6:55
4	0.39	0.38	0.37	6:09	6:07	6:05	-0.34	-0.39	-0.38	7:02	6:59	6:54
5	0.38	0.39	0.37	6:09	6:07	6:05	-0.33	-0.38	-0.37	6:59	6:56	10:33
6	0.36	0.36	0.35	6:06	6:05	6:03	-0.37	-0.37	-0.34	6:53	6:51	10:30
7	0.28	0.28	0.28	5:56	5:56	5:57	-0.26	-0.25	-0.25	6:41	6:41	10:23
8	0.30	0.30	0.30	5:58	5:58	5:59	-0.28	-0.30	-0.30	6:59	6:58	6:59
9	0.32	0.31	0.30	5:54	5:54	5:54	-0.27	-0.26	-0.25	10:10	6:58	6:59
10	0.32	0.32	0.31	5:55	5:55	5:54	-0.28	-0.27	-0.26	10:11	6:60	6:59
11	0.33	0.32	0.31	5:56	5:56	5:56	-0.34	-0.36	-0.37	10:13	7:01	6:59
12	0.41	0.42	0.41	6:10	6:10	6:07	-0.28	-0.29	-0.27	7:07	7:01	10:33

* Second wave is the highest

Table 4. Wave-induced current speeds (V) for the numerical simulations of the Alaska 1964 tsunami in Boundary Bay for the three sea level rise scenarios S1-S3. See Figures 20-21 for the site locations. The times for the occurrence of maximum wave-induced currents are in hours and minutes (HH:MM) after the start of the earthquake.

No	Maximum current speed (m/s)			Travel time to maximum current HH:MM		
	S1	S2	S3	S1	S2	S3
1	0.19	0.17	0.12	7:48	7:43	6:42
2	0.24	0.27	0.25	7:44	7:43	6:34
3	0.27	0.25	0.25	7:37	7:34	6:36
4	0.28	0.18	0.12	10:48	10:44	6:39
5	0.31	0.24	0.17	10:50	10:47	10:45
6	0.09	0.09	0.08	10:41	6:22	6:20
7	0.27	0.28	0.28	6:18	6:20	6:21
8	0.52	0.55	0.53	6:31	6:31	6:31
9	0.18	0.18	0.17	6:16	6:18	6:19
10	0.20	0.20	0.19	6:19	6:20	6:21
11	0.19	0.19	0.18	6:20	6:21	6:21
12	0.17	0.16	0.15	7:36	6:28	6:28

Table 5. Heights of present-day Dike and Higher High Water Mean Tide (HHWMT) along the shores of Boundary Bay for the cross-sections shown in Figure 9. Free-board = Height of Dike – HHWMT is the difference in elevation between the dike and the average higher high water levels during a year. S1 to S3 denote the three sea level rise Scenarios.

Section	Dike height (m)	Height of HHWMT (m)			Free-board (m)			Maximum wave height (m)		
		S1	S2	S3	S1	S2	S3	S1	S2	S3
A1	3.11	1.71	2.16	3.06	1.40	0.95	0.05	0.35	0.35	0.35
A2	3.42	1.71	2.16	3.06	1.71	1.26	0.36	0.36	0.37	0.35
B1	3.74	1.71	2.17	3.07	2.03	1.57	0.67	0.39	0.39	0.37
B2	3.68	1.71	2.17	3.07	1.97	1.50	0.59	0.37	0.38	0.37
C1	4.75	1.72	2.17	3.08	3.03	2.60	1.67	0.43	0.46	0.44
C2	2.75	1.72	2.17	3.08	1.03	0.60	-0.33	0.39	0.42	0.43

Comments:

Higher High Water Large Tide (HHWLT), which is the average highest water in a year, is 0.66 m higher than HHWMT for Point Atkinson and Vancouver.

The highest observed water level for Point Atkinson is 1.22 m above HHWMT, and for Vancouver it is 1.26 m above HHWMT.

4. CONCLUSIONS

A high-resolution, nested-grid tsunami model has been used to simulate the distribution of tsunami waves and wave-induced currents that will be generated in Boundary Bay during a 1964-type Alaska tsunami for three future sea level rise scenarios: S1, a 0.5 m global sea level rise scenario, corresponding to the median RCP8.5 model; S2, a 1.0 m global sea level rise scenario, corresponding to the upper RCP8.5 climate model; and S3, a 2.0 m global sea level rise, referred as the year 2200 model. The tsunami models use an advanced tsunami source distribution and high-resolution bathymetry for the area of interest. The major results of the modelling are:

- The initial conditions for scenarios S2 and S3 required an increase in the height of the dikes situated along the northern coast of Boundary Bay and along the Serpentine and Nicomekl rivers. Without an increase in dike elevation, flooding would have occurred in Scenarios S2 and S3 before any tsunami waves arrived in the study area (Table 5). Low-lying areas of the Campbell River valley would be flooded. Low lying areas in Greater Vancouver will also require added protection for global sea level rise Scenarios 2 and 3.
- The tsunami at Boundary Bay will reach heights of up to 0.45 m above the tidal level at the time of the wave arrivals for all scenarios (Table 3). The first wave will be the highest. Corresponding wave heights at Semiahmoo will be up to 0.35 m. For all sites in Boundary Bay, tsunami wave amplitudes only weakly depend on the initial sea level, and hence on the effect of global sea level rise.
- The distribution of tsunami wave amplitudes in Boundary Bay is non-uniform, with highest waves occurring toward the end of the bay (Mud Bay), and in Drayton Harbor; the distribution of wave amplitudes along the Semiahmoo coast is nearly uniform. Differences in the distribution of tsunami waves heights among the three sea level rise scenarios is small.
- The tsunami will induce moderate currents at the entrance to Drayton Harbor (up to 1.5 m/s), at the mouth of the Nicomekl River (up to 0.8 m/s) and at the mouth of the Campbell River (up to 0.7 m/s). With sea level rise, current speeds increase at the mouths of the rivers, but decrease at the entrance to Drayton Harbor.
- At Site 8, immediately south of the Nicomekl River near Mud Bay, the wave-induced current is up to 0.53 m/s for all scenarios, while for other sites, the current does not exceed 0.3 m/s for all sea level rise scenarios.

Because details of future tsunamis remain unknown in many aspects, we recommend the use of a safety factor of 50%, which should be added to the tsunami amplitudes estimated for a 1964-type event. However, even with such a large factor, the wave amplitudes from a Alaska 1964-type tsunami remain low compared to tidal variation or storm surge. The risk of flooding, however, certainly increases with increases in global sea level. Although the results of the tsunami modeling show that tsunami wave parameters are only weakly modified by the initial sea level, the arrival of

tsunami waves during times of future elevated initial sea levels will markedly increase the maximum water heights at the time of the tsunami.

ACKNOWLEDGEMENTS

This project was funded through “Coastal Flood Mitigation Canada” within the Defence Research and Development Canada’s Centre for Security Science (DRDC CSS) Program (CSSP), led on the Pacific Coast by Nicky Hastings of the Geological Survey of Canada, Natural Resources Canada. Her support, and that of our colleagues, throughout the program is gratefully acknowledged. We thank Tomas James (Natural Resources of Canada) for providing the digital sea level rise maps, Marlene Jeffries (Canadian Hydrographic Service) and Mark Rankin (Ocean Networks, Canada) for providing us with the high-resolution bathymetric and topographic data for the Boundary Bay region and for helping with the vertical datum adjustment. The authors gratefully thank Elena Suleimani (University of Alaska at Fairbanks) for providing us the latest source model for the Alaska 1964-type earthquake and tsunami. The penultimate version of this report was carefully edited and reformatted by Alexander Rabinovich. The final version was reviewed for publication by Neil Dangerfield of the Institute of Ocean Sciences (Fisheries and Oceans, Canada).

REFERENCES

Anderson, P. S., and Gow, G. A. (2004). *Tsunamis and Coastal Communities in British Columbia: An Assessment of the B.C. Tsunami Warning System and Related Risk Reduction Practices.*75xii pp. (Public Safety and Emergency Preparedness Canada, Ottawa, 2004).

British Columbia 3 arc-second Bathymetric Digital Elevation Model (2017). https://www.ngdc.noaa.gov/metaview/page?xml=NOAA/NESDIS/NGDC/MGG/DEM/iso/xml/4956.xml&view=getDataView&header=none.

Clague, J.J., Munro, A., and Murty, T.S. (2003). Tsunami hazard and risk in Canada, *Natural Hazards* 28 (2-3), 433-461.

Dunbar, D., LeBlond, P., and Murty, T.S. (1991). Evaluation of tsunami amplitudes for the Pacific coast of Canada. *Progress in Oceanography,* 26, 115-177.

Fine, I.V., Cherniawsky, J.Y., Rabinovich, A.B., and Stephenson, F.E. (2008). Numerical modeling and observations of tsunami waves in Alberni Inlet and Barkley Sound, British Columbia, Pure and Applied Geophysics, 165, (11/12), 2019-2044.l.

Fine, I.V., Thomson R.E., Lupton L.M., and Mundschutz, S. (2018a). Numerical Modelling of an Alaska 1964-type Tsunami at the Canadian Coast Guard Base in Seal Cove, British Columbia. *Canadian Technical Report of Hydrography and Ocean Sciences*, 321, Department of Fisheries & Oceans, Communications Directorate, Ottawa.

Fine, I.V., Thomson R.E., Lupton L.M., and Mundschutz, S. (2018b). Numerical Modelling of an Alaska 1964-type Tsunami at the Canadian Coast Guard Base in Victoria, British Columbia. *Canadian Technical Report of Hydrography and Ocean Sciences*, 323, Department of Fisheries & Oceans, Communications Directorate, Ottawa.

GEBCO One Minute Grid, The. Version 2.0 (2014). http://www.gebco.net.

Johnson, J.M., Satake, K., Holdahl, S.R., and Sauber, J. (1996). The 1964 Prince William Sound earthquake— Joint inversion of tsunami waveforms and geodetic data. *Journal of Geophysical Research*, 101, no. B1, p. 523–532.

Lander, J.F. (1996). *Tsunamis Affecting Alaska, 1737-1996*. Boulder, CO: U.S. Department of Commerce.

Myers, E.P., and Baptista, A.M. (2001). Analysis of Factors Influencing Simulations of the 1993 Hokkaido Nansei-Oki and 1964 Alaska Tsunamis. *Natural Hazards* (2001) 23: 1. https://doi.org/10.1023/A:1008150210289.

NOAA (2017). *British Columbia, 3 arc-second MSL DEM*. https://www.ngdc.noaa.gov/dem/squareCellGrid/download/4956. Last access on 11.10.2017.

National Tsunami Hazard Mapping Program (NTHMP) (2010). *Guidelines and Best Practices for Tsunami Inundation Modeling for Evacuation Planning*. NTHMP Mapping & Modeling Subcommittee, NOAA, USA.

Spaeth, M.G., and Berkman, S.C. (1967). The tsunami of March 28, 1964, as recorded at tide stations. *Coast and Geod. Survey Techn. Bull*. 33, US Department of Commerce, 86 p.

Suito, H., and Freymueller, J.T. (2009). A viscoelastic and afterslip post seismic model for the 1964 Alaska earthquake. *Journal of Geophysical Research*, 114, B11404, doi:10.1029/2008JB005954.

Suleimani, E.N. (2011). *Numerical studies of tectonic and landslide-generated tsunamis caused by the 1964 Great Alaska Earthquake*. Fairbanks, Alaska, University of Alaska Fairbanks, Ph.D. dissertation, 181 p.

Suleimani, E.N., and Freymueller, J.T. (2020). Near-field modeling of the 1964 Alaska tsunami: The role of splay faults and horizontal displacements. *Journal of Geophysical Research: Solid Earth,* doi:10.1029/2020jb019620.